Synthesis and bioevaluation of novel stilbene-based derivatives as tubulin/HDAC dual-target inhibitors with potent antitumor activities in vitro and in vivo

Huajian Zhu[a,†], Wenjian Zhu[a,†], Yang Liu[a], Tian Gao[a], Jingjie Zhu[a], Yuchen Tan[a], Han Hu[a], Wenhao Liang[a], Lingyue Zhao[a], Jian Chen[b], Zheying Zhu[c], Jichao Chen[d,*], Jinyi Xu[a,*], Shengtao Xu[a,b,*]

[a] State Key Laboratory of Natural Medicines and Department of Medicinal Chemistry, China Pharmaceutical University, 24 Tong Jia Xiang, Nanjing 210009, P. R. China

[b] Department of Hepatobiliary Surgery, The First People's Hospital of Kunshan, Suzhou, 215132, P. R. China

[c] Division of Molecular Therapeutics & Formulation, School of Pharmacy, The University of Nottingham, University Park Campus, Nottingham NG7 2RD, UK

[d] School of Pharmacy, Nanjing University of Chinese Medicine, Nanjing, China

[†] These authors contributed equally to this work.

* Corresponding authors e-mail address: jinyixu@china.com (Jinyi Xu); cpuxst@cpu.edu.cn (Shengtao Xu); chenjichao@njucm.edu.cn (Jichao Chen)

Abstract

A series of novel stilbene-based derivatives were designed and synthesized as tubulin/HDAC dual-target inhibitors. Among forty-three target compounds, compound **II-19k** not only exhibited considerable antiproliferative activity in the hematological cell line K562 with IC_{50} value of 0.003 μM, but also effectively inhibited the growth of various solid tumor cell lines with IC_{50} values ranging from 0.005 to 0.036 μM. The mechanism studies demonstrated that **II-19k** could inhibit microtubules and HDACs at the cellular level, block cell cycle arrest at G2 phase, induce cell apoptosis, and reduce solid tumor cells metastasis. What's more, the vascular disrupting effects of compound **II-19k** were more pronounced than the combined administration of parent compound **8** and HDAC inhibitor SAHA. The *in vivo* antitumor assay of **II-19k** also showed the superiority of dual-target inhibition of tubulin and HDAC. **II-19k** significantly suppressed the tumor volume and effectively reduced tumor weight by 73.12% without apparent toxicity. Overall, the promising bioactivities of **II-19k** make it valuable for further development as an antitumor agent.

Keywords: Stilbene, Dual-target inhibitors, Tubulin, HDAC, Antitumor

1. Introduction

Due to the heterogeneity and adaptivity of tumors, the single target antitumor drugs usually suffer from some drawbacks including transitory clinical efficacy, inevitable drug resistance and relapses [1-3]. The combination therapies like multicomponent drug cocktails have been intensively developed to improve antitumor efficacies. However, the poor patient compliance, unpredictable pharmacokinetics and pharmacodynamics, and drug-drug interactions may present unacceptable risks for tumor combination therapies in clinical [4-6]. With deep understanding of tumor pathogenesis, the strategy "polypharmacology drugs", a single molecule simultaneously targets multiple mechanisms of cancer, is emerging as a new paradigm in drug discovery, which could address these limitations associated with the single-target or combination tumor therapies [7, 8].

Epigenetic enzymes play an important role in tumorigenesis and development. Among them, histone deacetylases (HDACs) regulate the architecture and function of oncogenes and apoptotic genes by removing the acetyl group of histones and nonhistone proteins. The overexpression of HDACs is involved in tumor proliferation, migration, apoptosis, and angiogenesis, and thus, they are regarded as promising therapeutic targets for cancer [9, 10]. There are now five HDAC inhibitors approved by the regulatory agencies for cancer therapy, namely vorinostat (SAHA, **1**), romidepsin (**2**), belinostat (**3**), chidamide (**4**), and panobinostat (**5**). The vast majority of HDAC inhibitors have a well-defined pharmacophore model, containing surface recognition cap group, linker, and zinc ion binding group (ZBG), respectively (Figure 1). Nevertheless, it's noteworthy that most of HDAC inhibitors, despite their great success in the treatment of hematological malignancies, have not shown significant clinical benefits as single agents in solid tumors. The development of HDAC-based multitarget inhibitors is assumed as a potent and attractive solution to this dilemma [11-13]. Recently, some studies have shown that the synergistic antitumor effects on solid tumors can be achieved by the combination of microtubule polymerization inhibitors and HDAC inhibitors [14-18], suggesting that the design of tubulin/HDAC hybrid inhibitors should be a reasonable strategy for the treatment of solid tumors.
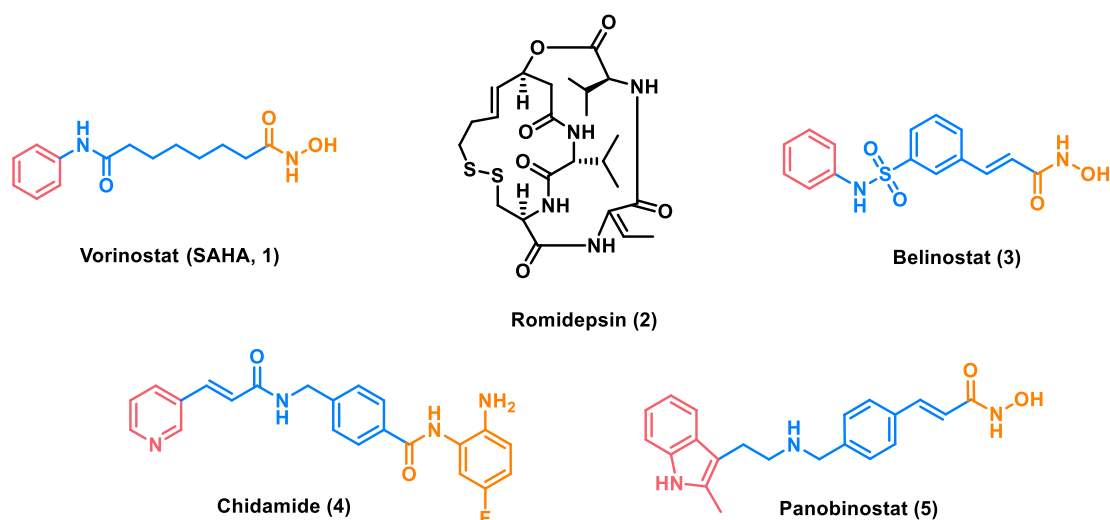

Figure 1. Chemical structures of marketed HDAC inhibitors. The three sections of HDAC inhibitor pharmacophore are shown in three different colors. Pink: cap group; blue: linker; orange: ZBG.

Microtubules consist mainly of α, β-tubulin heterodimers that serve as cytoskeletal filaments in eukaryotes [19]. More than six drug binding sites such as taxane, laulimalide, vinca alkaloid, pironetin, colchicine and maytansine have been identified in microtubules. The agents binding to the site like taxane or laulimalide act as tubulin stabilizers to promote microtubule polymerization, while those agents binding to the site like colchicine or pironetin act as tubulin destabilizers to inhibit microtubule polymerization [20, 21]. Attracted by the intrinsic properties including but not limited to structural simplicity, wide therapeutic window, vascular destruction ability and low toxicity, medicinal chemists have conducted considerable research on colchicine binding site inhibitors (CBSIs) in recent years [22, 23]. Structurally, combretastatin A-4 (CA-4, **6**) is one of the simplest CBSIs, which makes it the subject of many structural modifications. However, the fatal flaw of chemical instability, easy isomerization to the inactive but thermodynamically stable *E*-isomer, limits the clinical application of CA-4 [24-26]. Stilbene is considered as a privileged skeleton for the modifications of CA-4 with desirable chemical and metabolic stability. The stilbene-based derivative *iso*CA-4 (**7**) have equivalent antitumor properties as CA-4 but without the risk of isomerization [27]. Alami *et al*. reported a stilbene analog **8** with a quinoline fragment in place of the 3,4,5-trimethoxyphenyl ring (ring A) present in *iso*CA-4, which displayed potent antiproliferative activities against a panel of cancer cell lines [28]. On this basis, our group further replaced isovanillin with the indole ring (ring B) to afford stilbene analog **9** (Figure 2). The *in vitro* and *in vivo* studies showed that analog **9** exhibited prominent antitumor activities and low toxicity [29].
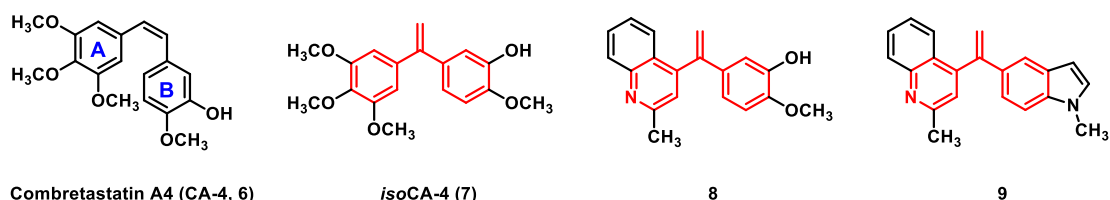

Figure 2. Chemical structures of CA-4 and its stilbene analogs.

Recently, we reported a series of *N*-benzylbenzamide based tubulin/HDAC dual-

target inhibitors that more effectively inhibit the growth of solid tumors by targeting internal and peripheral tumor vessels [14]. In a continuation of our interest in developing novel tubulin/HDAC hybrid inhibitors, we designed a novel series of stilbene-based derivatives as tubulin/HDAC dual-target inhibitors by introducing ZBG to the structures of potent analogs **8** and **9**. Through the molecular docking analysis, it could be seen that the orientations of the methyl group on pyridine (ring A) and the hydroxyl group on the benzene ring (ring B) have a certain space for the further structural modification, which are suitable sites to introduce linker and ZBG, respectively (Figure 3). Herein, a total of forty-three target compounds were designed, synthesized and assayed for antiproliferative activities against hematological malignancies and solid tumor cell lines, along with the analysis of structure-activity relationships (SARs) analysis. The comprehensive activity evaluation identified optimal compound **II-19k** with balanced HDAC and tubulin inhibitory activities, desirable *in vitro* antiproliferation profiles, potent anti-vascular potency, and *in vivo* antitumor efficacy.
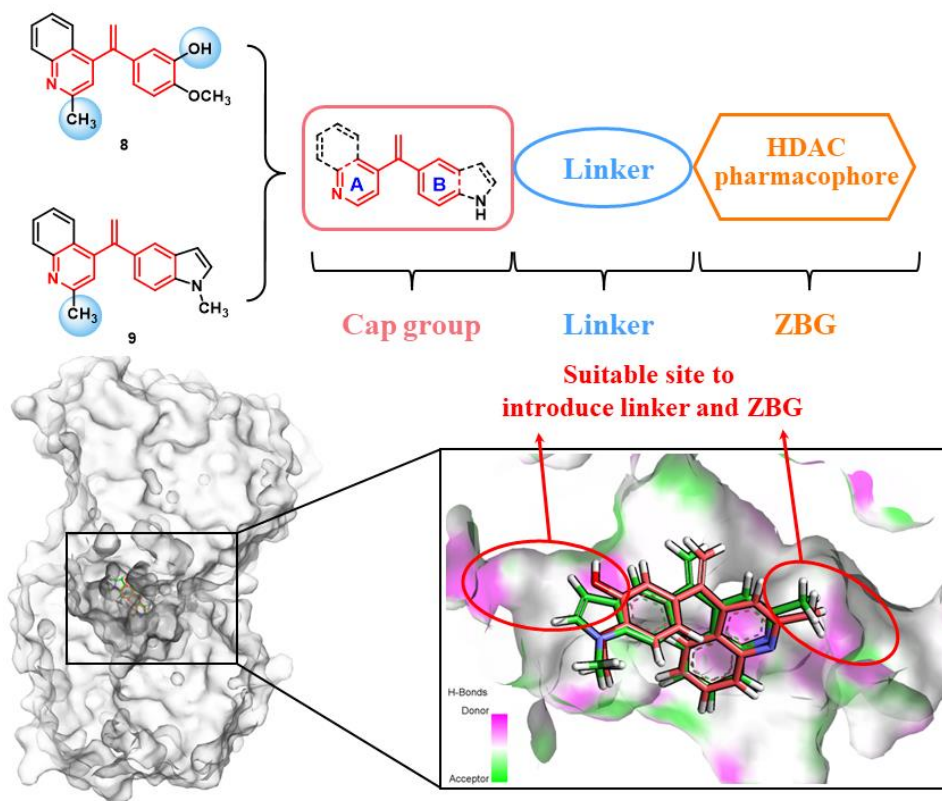

Figure 3. Rational design of stilbene-based tubulin/HDAC dual-target inhibitors. The

binding mode of stilbene analogs **8** and **9** in the active site of tubulin (PDB ID: 5 LYJ). Compound **8** is colored in pink, and compound **9** is colored in green. The figures were generated using PyMol (http://www.pymol.org).

2. Results and discussion

### 2.1. Synthesis of Target Stilbene-based Derivatives

The chemical synthesis of stilbene-based intermediates **S4a~i** was performed according to the procedures in Scheme 1. In general, different substituted acetophenones **S1a~e** reacted with *p*-toluenesulfonhydrazide to afford their corresponding *p*-toluenesulfonylhydrazone intermediates **S2a~e.** Then, these intermediates were coupled with 4-chloroquinoline derivatives **S3a~b** or 4-chloropyridine derivatives **S3c~e** via Pd-catalyzed cross coupling reactions to afford compounds **S4a~i**.
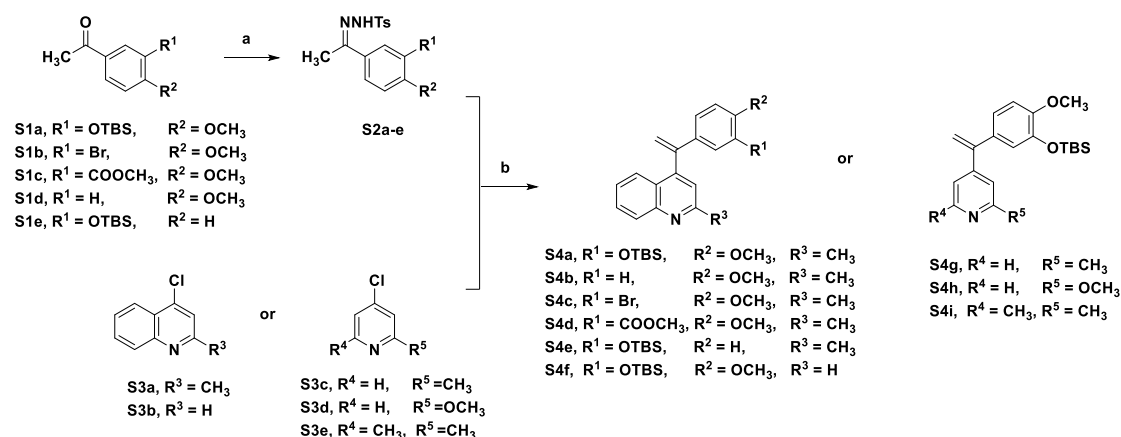
Scheme 1. Reagents and conditions: (a) *p*-toluenesulfonhydrazide, EtOH, 90 °C, 4 h, 80-90%; (b) PdCl$_2$(CH$_3$CN)$_2$, Xphos, *t*-BuOLi, 1,4-dioxane, 100 °C, 2-10 h, 23-86%.

The *N*-1 of 5-acetylindole was protected to afford *N*-Boc-5-acetylindole **S6**, which was then coupled following the procedures as described above to yield compound **S8**. The methyl side chain of compound **S8** was oxidized with selenium dioxide in 1,4-dioxane to provide the required aldehyde **S9** (Scheme 2). The syntheses of target compounds **I-12a~c** bearing indole moieties were also described in Scheme 2. The Witting reaction of compound **S9** with ethyl 2-(diethoxyphosphoryl)acetate led to **S10a**,

which was deprotected by trifluoroacetic acid and hydrolyzed with hydroxylamine to yield target compound **I-12a**. The oxidation of **S9** could yield carboxylic acid **S10b**, which was then subjected to amide condensation and deprotection to obtain target compound **I-12b**. In addition, the reduction of **S9** by sodium borohydride could yield alcohol **S10c**. Compound **S10c** was converted to **S11c** via the Williamson ether synthesis. The following deprotection of the Boc group afforded **S11d**, which was subsequently reacted with NH2OK to give target compound **I-12c**. As shown in Scheme 3, target compounds **I-12d~i** were prepared in a similar manner as described above.
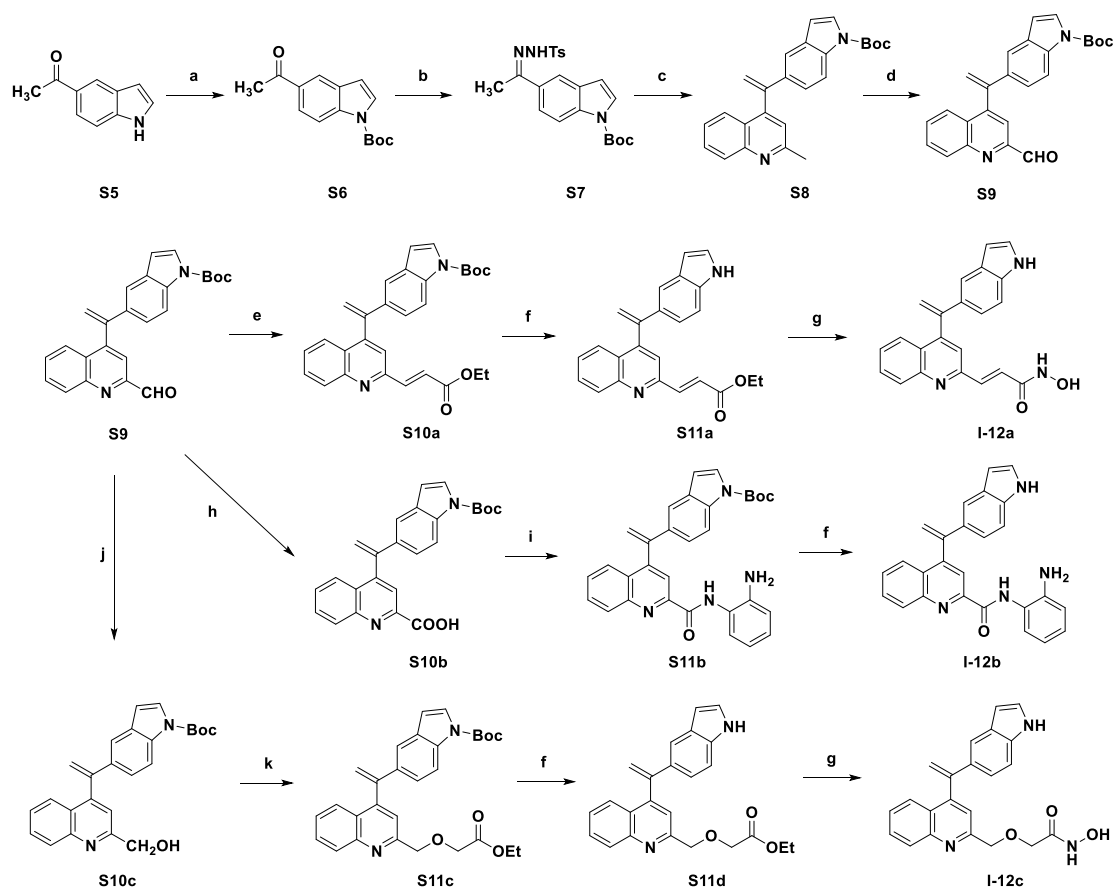
Scheme 2. Reagents and conditions: (a) NaH, (Boc)2O, THF, rt, 30 min; MeOH, 30 min, 62%; (b) *p*-toluenesulfonhydrazide, EtOH, 90 °C, 4 h, 81%; (c) PdCl2(CH3CN)2, Xphos, *t*-BuOLi, 1,4-dioxane, 100 °C, 8 h, 47%; (d) SeO2, 1,4-dioxane, 100 °C, 1 h, quantitative yield; (e) ethyl 2-(diethoxyphosphoryl)acetate, NaH, THF, Ar, 0 °C to reflux, 1 h, 93%; (f) TFA, DCM, rt, 3 h, quantitative yield; (g) NH2OH·HCl, MeOH, rt, 30 min, 57-70%; (h) NaClO2, NaH2PO4, 2-methyl-2-butene, *t*-BuOH, H2O, rt, 2 h, quantitative yield; (i) benzene-1,2-diamine, EDCI, TEA, DCM, rt, overnight, 47%; (j)

NaBH$_4$, THF, rt, 30 min, 85%; (k) NaH, BrCH$_2$COOEt, THF, 0 °C to rt, overnight, 87%.
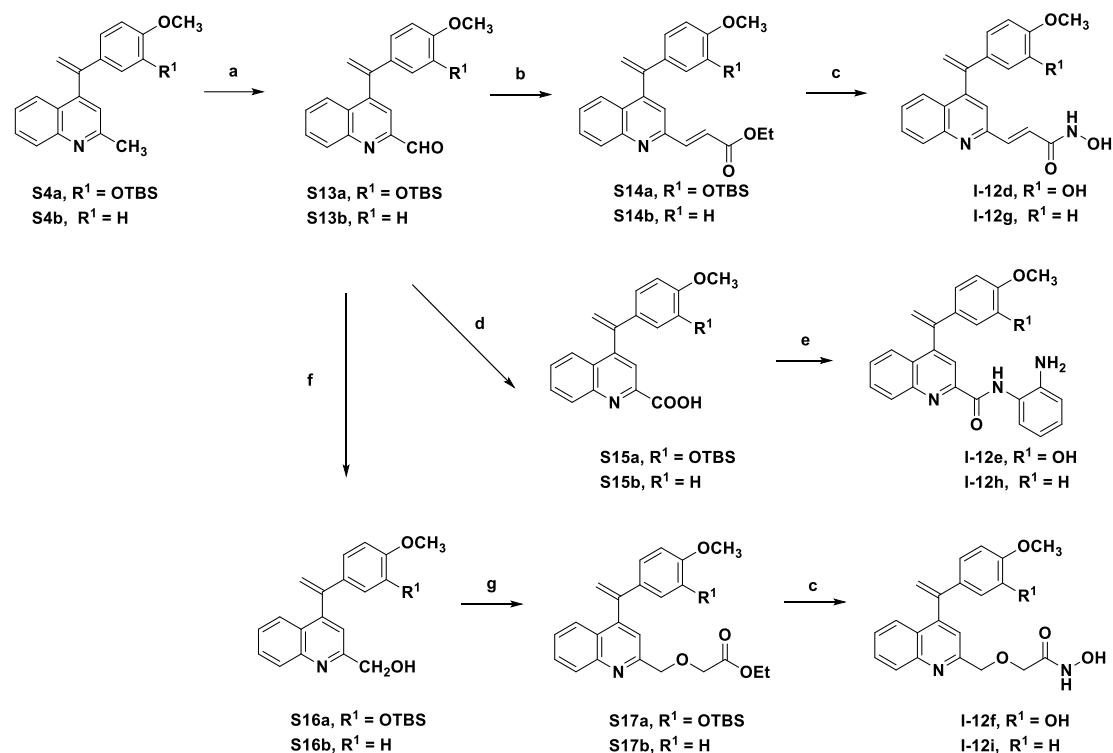
Scheme 3. Reagents and conditions: (a) SeO$_2$, 1,4-dioxane, 100 °C, 1 h, quantitative yield; (b) ethyl 2-(diethoxyphosphoryl)acetate, NaH, THF, Ar, 0 °C to reflux, 1 h, 78%; (c) 1) for derivatives with TBS protecting groups: TBAF, THF, rt, 20 min, quantitative yield; 2) NH$_2$OH·HCl, MeOH, rt, 30 min, 45-60%; (d) NaClO$_2$, NaH$_2$PO$_4$, 2-methyl-2-butene, t-BuOH, H$_2$O, rt, 2 h, 73%; (e) 1) for derivatives with TBS protecting groups: TBAF, THF, rt, 20 min, quantitative yield; 2) benzene-1,2-diamine, EDCI, TEA, DCM, rt, overnight, 30%; (f) NaBH$_4$, THF, rt, 30 min, 67%; (g) NaH, BrCH$_2$COOEt, THF, 0 °C to rt, overnight, 63%.

The synthetic routes of target compounds **II-19a~v** and **II-25a~l** were depicted in Scheme 4. Bromobenzene intermediate **S4c** reacted with methyl acrylate using Heck coupling to afford acrylate derivative **S18**, which could be transformed to hydroxamic acid **II-19a**. Intermediate **S4d** could be directly converted into hydroxamic acid **II-19b** by NH$_2$OK in methanol. Besides, hydrolysis of intermediate **S4d** followed by condensation with 1,2-diaminobenzene led to *ortho*-aminoanilide **II-19c**. The intermediates **S4a** and **S4e~i** were deprotected using tetrabutylammonium fluoride

(TBAF) in THF to give compounds **S21a**, **e**, **f** and **S23g~i**. These derivatives with hydroxyl groups underwent Williamson ether synthesis to produce corresponding ester intermediates, which subsequently reacted with NH$_2$OK/methanol solution to give hydroxamic acid compounds **II-19a~v** and **II-25a~l** (specific structures depicting in Tables 2 and 3).
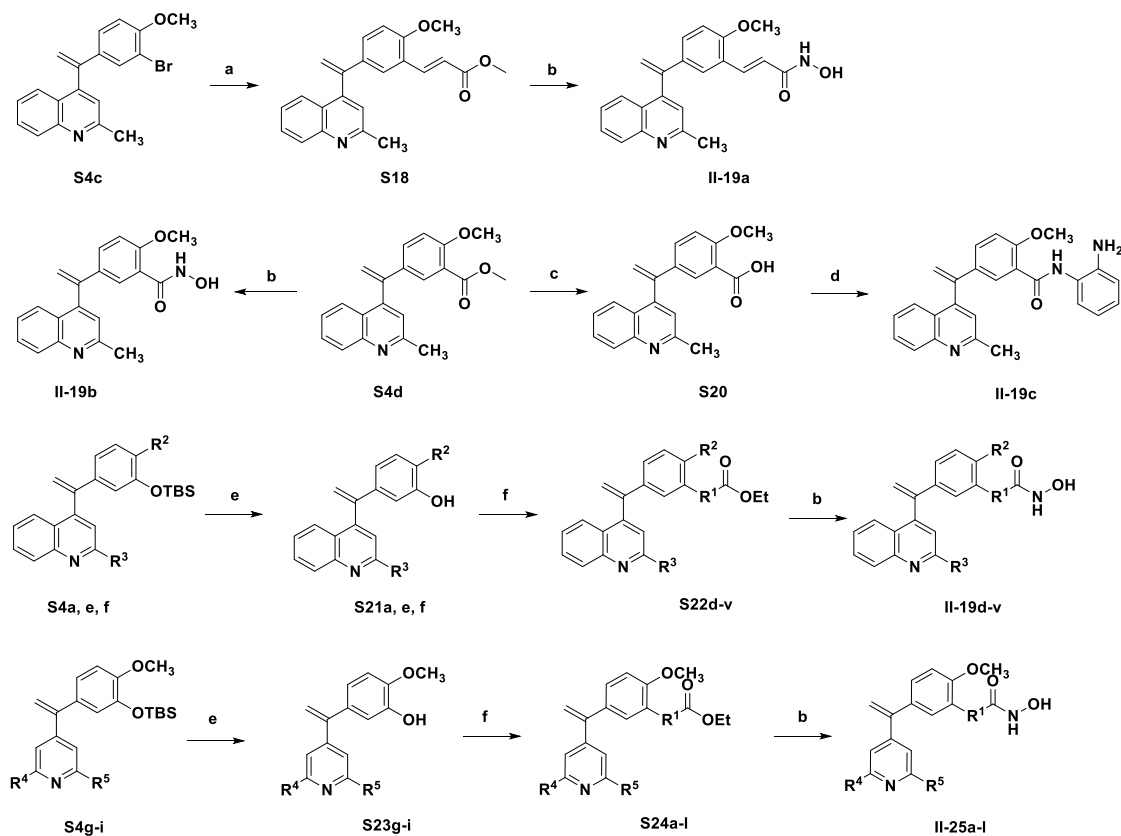
Scheme 4. Reagents and conditions: (a) methyl acrylate, Pd(PPh$_3$)$_2$Cl$_2$, TEA, DMF, Ar, 160 °C, overnight, 50%; (b) NH$_2$OH·HCl, MeOH, rt, 10 min-12 h, 20-67%; (c) NaOH, THF, 40 °C, overnight, quantitative yield; (d) benzene-1,2-diamine, EDCI, DIPEA, HOBT, DMF, rt, 2 h, 71%; (e) TBAF, THF, rt, 10 min, quantitative yield; (f) Cs$_2$CO$_3$, TBAI, Br(CH$_2$)$_n$COOEt, CH$_3$CN, reflux, 30 min-2 h, quantitative yield.

2.2 Antiproliferative Activities and SARs

In the first-round modification, we investigated the SARs of the different ring B and ZBG substitutions on the ring A. The antiproliferative activities of target compounds **I-12a~i** were preliminarily evaluated in human chronic myelogenous leukemia K562 cells using MTT assay, with CA-4 as the positive control. The results in Table 1

suggested that compounds with 3-hydroxy-4-methoxy phenyl as ring B exhibited the most potent activity at 1 μM concentration. While the replacement of ring B with indole or 4-methoxy phenyl led to a decrease or loss of activity. Compounds bearing *ortho*-phenylenediamine-based ZBG (**I-12b**, **e** and **h**) produced no antiproliferative effects regardless of different substitutions of ring B. The *N*-hydroxyacrylamide group, a privileged structure used by many potent HDAC inhibitors such as the approved drug panobinostat and belinostat, showed the superiority in the antiproliferative potency (**I-12d** and **g**).

Table 1. *In vitro* inhibitory rates of target compounds **I-12a~i** on K562 cells.
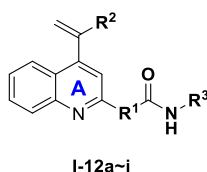
Compd.	R^1	R^2	R^3	Inhibition Rate of K562 (%)^a		
				@1 μM	@0.1 μM	@0.01 μM
I-12a	CH=CH	indole (NH)	OH	4.78	3.73	3.16
I-12b	-	indole (NH)	2-aminophenyl	2.75	2.75	-0.17
I-12c	CH$_2$OCH$_2$	indole (NH)	OH	14.96	6.23	2.28
I-12d	CH=CH	OCH$_3$/OH phenyl	OH	87.27	12.90	-0.17
I-12e	-	OCH$_3$/OH phenyl	2-aminophenyl	4.26	3.71	0.16
I-12f	CH$_2$OCH$_2$	OCH$_3$/OH phenyl	OH	71.46	6.41	0.83
I-12g	CH=CH	OCH$_3$ phenyl	OH	43.51	6.82	1.41
I-12h	-	OCH$_3$ phenyl	2-aminophenyl	1.10	0.24	-0.16
I-12i	CH$_2$OCH$_2$	OCH$_3$ phenyl	OH	39.98	3.00	2.60
CA-4	-	-	-	95.05	88.38	86.59

^{a}The data were expressed as the mean of two independent experiments.

In the second-round of optimization, we further investigated the effect of ZBG attachment at the ring B on the antiproliferative activity. Compound **II-19a** with *N*-hydroxycinnamamide fragment displayed potent inhibitory activity with an IC_{50} value of 0.042 μM. The direct attachment of hydroxamic moiety to C-3 position of ring B (**II-19b**) led to a drop in the activity. The inhibitory activity against K562 cells was greatly decreased when the hydroxamic acid group of the compound **II-19b** was replaced by *ortho*-aminoanilide (**II-19c**). Comparing the cytotoxic data of compounds **II-19e~h** with that of compound **II-19d**, it is obvious to figure out that the extension of linker had a detrimental influence on antiproliferative activities. A similar trend was observed on derivatives **II-19m~v**. The introduction of the methyl into the linker of compound **II-19d** was well tolerated (**II-19i** and **j**). Besides, compound **II-19k** with a fluoro substituent on the linker displayed the best antiproliferative potency with an IC_{50} value of 0.003 μM. However, the introduction of an additional fluorine atom into the linker (**II-19l**) resulted in decreased activity dramatically. When the methoxy group of ring B was removed, the IC_{50} value decline to 2.479 μM for compound **II-19m**, indicating the importance of the methoxy group to the activity. In contrast to **II-19d**, compound **II-19s**, in which the methyl group of ring A was changed to an H atom, had a 10-fold decrease in inhibition activity. What's more, different substituted pyridine derivatives **II-25a~l** were synthesized and evaluated for their antiproliferative activity (Table 3). However, the activities of this series decreased to varying degrees compared with those of corresponding quinoline derivatives. In addition, compounds **8** (IC_{50} = 1.8 nM) and **9** (IC_{50} = 2 nM) exhibited similar antiproliferative activities as compound **II-19k** on K562 cancer cells [28-29], whereas the activity of SAHA was comparatively poor (IC_{50} = 444 nM) [30].

Table 2. *In vitro* antiproliferative activities of target compounds **II-19a~v** on K562 cells.
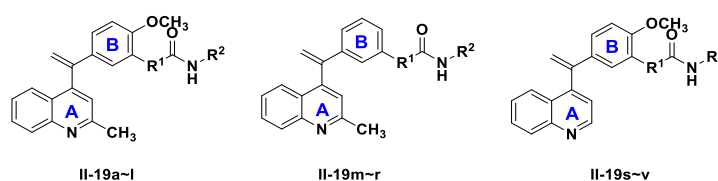
Compd.	R_1	R_2	K562 IC$_{50}$ values (μM)[a]	Compd.	R_1	R_2	K562 IC$_{50}$ values (μM)[a]
II-19a	CH=CH	OH	0.042 ± 0.004	**II-19m**	OCH$_2$	OH	2.479 ± 0.149
II-19b	-	OH	1.318 ± 0.053	**II-19n**	OCH(CH$_3$)	OH	2.367 ± 0.142
II-19c	-	2-aminophenyl	22.226 ± 1.334	**II-19o**	OC(CH$_3$)$_2$	OH	6.864 ± 0.206
II-19d	OCH$_2$	OH	0.008 ± 0.001	**II-19p**	O(CH$_2$)$_3$	OH	3.002 ± 0.182
II-19e	O(CH$_2$)$_2$	OH	0.061 ± 0.006	**II-19q**	OCH$_2$CH=CH	OH	2.743 ± 0.165
II-19f	O(CH$_2$)$_3$	OH	0.173 ± 0.019	**II-19r**	O(CH$_2$)$_5$	OH	9.271 ± 0.556
II-19g	O(CH$_2$)$_4$	OH	1.835 ± 0.074	**II-19s**	OCH$_2$	OH	0.079 ± 0.011
II-19h	O(CH$_2$)$_5$	OH	2.259 ± 0.115	**II-19t**	OCH(CH$_3$)	OH	0.069 ± 0.007
II-19i	OCH(CH$_3$)	OH	0.007 ± 0.001	**II-19u**	O(CH$_2$)$_3$	OH	1.461 ± 0.058
II-19j	OC(CH$_3$)$_2$	OH	0.005 ± 0.001	**II-19v**	O(CH$_2$)$_5$	OH	3.336 ± 0.135
II-19k	OCHF	OH	0.003 ± 0.001	**CA-4**	-	-	0.007 ± 0.001
II-19l	OCF$_2$	OH	0.204 ± 0.013				

[a]IC$_{50}$ values are indicated as the mean ± SD of three independent experiments.

Table 3. *In vitro* antiproliferative activities of target compounds **II-25a~l** on K562 cells.
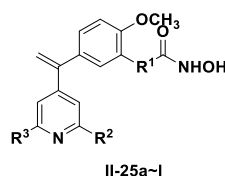
II-25a~l

Compd.	R^1	R^2	R^3	K562 IC$_{50}$ values (μM)[a]	Compd.	R^1	R^2	R^3	K562 IC$_{50}$ values (μM)[a]
II-25a	OCH$_2$	CH$_3$	H	0.107 ± 0.014	**II-25h**	O(CH$_2$)$_5$	OCH$_3$	H	3.855 ± 0.185
II-25b	OCH(CH$_3$)	CH$_3$	H	0.060 ± 0.008	**II-25i**	OCH$_2$	CH$_3$	CH$_3$	0.026 ± 0.003
II-25c	O(CH$_2$)$_3$	CH$_3$	H	1.487 ± 0.089	**II-25j**	OCH(CH$_3$)	CH$_3$	CH$_3$	0.019 ± 0.001
II-25d	O(CH$_2$)$_5$	CH$_3$	H	2.875 ± 0.172	**II-25k**	O(CH$_2$)$_3$	CH$_3$	CH$_3$	0.516 ± 0.019
II-25e	OCH$_2$	OCH$_3$	H	0.055 ± 0.004	**II-25l**	O(CH$_2$)$_5$	CH$_3$	CH$_3$	1.919 ± 0.096
II-25f	OCH(CH$_3$)	OCH$_3$	H	0.061 ± 0.002	CA-4	-	-	-	0.007 ± 0.001
II-25g	O(CH$_2$)$_3$	OCH$_3$	H	1.136 ± 0.071					

[a]IC$_{50}$ values are indicated as the mean ± SD of three independent experiments.

Since these newly stilbene derivatives possessed remarkable antiproliferative activities against K562 cells, we tended to further evaluate the cytotoxic activities of the representative compounds against solid tumor cell lines including breast carcinoma

cells MCF-7 and MDA-MB-231, non-small cell lung cancer cell A549, melanoma cell B16F10, ovarian cancer cell A2780, and one human normal fetal lung fibroblast 1 (HFL-1) cell line. As shown in Table 4, these selected dual-target inhibitors could effectively inhibit the growth of the solid tumor cells in nanomolar ranges, especially **II-19k** had the IC_{50} values between 0.005 to 0.036 μM, which showed comparable or even better antiproliferative activities than those of CA-4. In addition, all these compounds exhibited relatively low cytotoxicity against normal cell HFL-1, indicating that these stilbene-based hybrid inhibitors might have low toxicity.

Table 4. Antiproliferative activities of representative compounds against five cancer cell lines and normal human lung cells.

Compd.	IC_{50} values (μM)[a]					
	MCF-7	MDA-MB-231	A549	B16F10	A2780	HFL-1
II-19a	0.017 ± 0.002	0.011 ± 0.001	0.009 ± 0.001	0.015 ± 0.002	0.005 ± 0.001	0.311 ± 0.022
II-19d	0.055 ± 0.004	0.032 ± 0.003	0.038 ± 0.003	0.028 ± 0.002	0.016 ± 0.002	0.195 ± 0.012
II-19i	0.022 ± 0.002	0.028 ± 0.003	0.015 ± 0.002	0.030 ± 0.003	0.014 ± 0.001	0.095 ± 0.006
II-19j	0.044 ± 0.005	0.031 ± 0.003	0.009 ± 0.001	0.004 ± 0.001	0.008 ± 0.001	0.103 ± 0.008
II-19k	0.036 ± 0.002	0.011 ± 0.001	0.017 ± 0.002	0.005 ± 0.001	0.005 ± 0.001	0.230 ± 0.014
II-25i	0.052 ± 0.004	0.111 ± 0.008	0.069 ± 0.005	0.098 ± 0.008	0.036 ± 0.003	0.264 ± 0.016
II-25j	0.019 ± 0.002	0.099 ± 0.007	0.080 ± 0.006	0.072 ± 0.006	0.023 ± 0.003	0.213 ± 0.013
CA-4	0.071 ± 0.006	0.029 ± 0.003	0.002 ± 0.001	0.007 ± 0.001	0.003 ± 0.001	0.082 ± 0.005

[a]IC_{50} values are indicated as the mean ± SD of three independent experiments.

2.3 In Vitro Inhibition Potencies against HDACs

In consideration of the prominent antiproliferative activities of these target

compounds against various cancer cells, we next investigated their HDACs inhibitory potencies using HeLa nuclear extract with SAHA as the positive control. The results in Table 5 revealed that, when the ZBG was linked to ring A (**I-12a~i**), the compounds with hydroxamic acid had better HDAC inhibition activity. The introduction of a longer linker between the parent nucleus and ZBG was conducive to HDACs inhibitory potencies, which showed an opposite trend from that observed in the antiproliferative activities against cancer cells. The modification of ring A or ring B had no dramatic influence on the HDACs activities. Comprehensively considering the antiproliferative activities and HDAC inhibitory activities, we chosen compound **II-19i** and **II-19k** for HDAC isoenzymes inhibition assays. The results in Table 6 showed that the fluoro substituent on the linker made the inhibitory activities of compound **II-19k** against HDAC isoforms significantly greater than those of compound **II-19i**. Compound **II-19k** possessed potent inhibition toward HDAC1/2/6, but relatively lower activity against HDAC3. Moreover, both target compounds showed very poor inhibitory activities against HDAC7, with IC_{50} values of larger than 10 μM. Based on the above results, compound **II-19k** was selected for subsequent study.

Table 5. Inhibitory potencies of target compounds against HDACs.

Compd.	HDACs Inh (%)[a]		Compd.	HDACs Inh (%)[a]		Compd.	HDACs Inh (%)[a]	
	@10 μM	@ 1 μM		@10 μM	@ 1 μM		@10 μM	@ 1 μM
I-12a	75	15	**II-19g**	95	74	**II-19v**	94	82
I-12b	5	0	**II-19h**	97	87	**II-25a**	27	10
I-12c	74	36	**II-19i**	68	37	**II-25b**	57	27
I-12d	93	76	**II-19j**	35	7	**II-25c**	97	86
I-12e	12	4	**II-19k**	87	65	**II-25d**	100	96
I-12f	84	66	**II-19l**	46	15	**II-25e**	35	0
I-12g	64	17	**II-19m**	92	75	**II-25f**	22	8
I-12h	8	6	**II-19n**	54	24	**II-25g**	97	88
I-12i	87	54	**II-19o**	25	3	**II-25h**	96	92
II-19a	34	6	**II-19p**	96	82	**II-25i**	2	2
II-19b	34	13	**II-19q**	93	84	**II-25j**	33	3
II-19c	2	1	**II-19r**	92	54	**II-25k**	92	66
II-19d	40	5	**II-19s**	51	14	**II-25l**	99	64
II-19e	17	6	**II-19t**	13	7	SAHA	99	98

| II-19f | 95 | 70 | II-19u | 94 | 77 |

Table 6. *In vitro* inhibition of HDAC subtype for selected compounds.

Compd.	IC$_{50}$ values (μM)[a]				
	HDAC1	HDAC2	HDAC3	HDAC6	HDAC7
II-19i	1.465 ± 0.037	2.318 ± 0.041	8.910 ± 0.310	4.682 ± 0.390	>10
II-19k	0.403 ± 0.020	0.591 ± 0.035	3.552 ± 0.184	0.459 ± 0.026	>10
SAHA	0.048 ± 0.002	0.208 ± 0.012	0.052 ± 0.003	0.025 ± 0.001	0.082 ± 0.005

[a]IC$_{50}$ values are indicated as the mean $\pm$ SD of three independent experiments.

2.4 Tubulin Polymerization by Binding to the Colchicine Binding Site

To investigate whether these dual-target compounds interacted with tubulin system, the representative compound **II-19k** was selected to evaluate the inhibitory effects on tubulin polymerization *in vitro* with CA-4 as the reference compound. As shown in Figure 4, paclitaxel, as a microtubule-stabilizing agent, increased the absorbance obviously, indicating that it could enhance tubulin polymerization. While compound **II-19k** decreased the absorbance in a concentration-dependent manner, which was consistent with the effect of the microtubule depolymerizing agent CA-4. Next, the IC$_{50}$ value of **II-19k** in inhibiting tubulin polymerization was determined as shown in Table 7. The results showed that compound **II-19k** (IC$_{50}$ = 3.84 μM) exhibited slightly less potent tubulin polymerization inhibitory activity than that of CA-4 (IC$_{50}$ = 2.01 μM). In addition, compound **II-19k** was evaluated for potential inhibition of [^{3}H]-colchicine binding to tubulin. The binding potency of compound **II-19k** to colchicine binding site was 64.43% at the concentration of 5 μM, suggesting that compound **II-19k** inhibited microtubule polymerization by binding to the colchicine binding site.
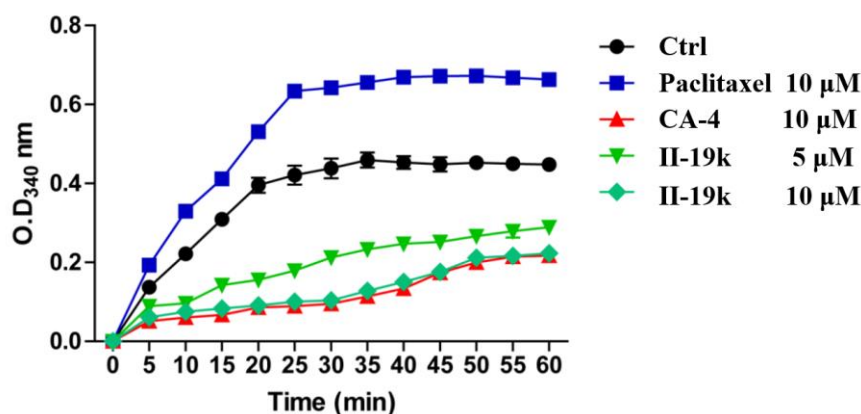
Figure 4. The *in vitro* effects **II-19k** on tubulin polymerization were measured by monitoring the absorbance at 340 nm every 5 minutes for 60 minutes at 37 °C. The experiments were repeated thrice.

Table 7. Inhibition of tubulin polymerization and colchicine binding to tubulin[a].

Compd.	inhibition of tubulin polymerization	inhibition of colchicine binding (%) inhibition ± SD[b]	
	IC$_{50}$ (μM)	1 μM	5 μM
II-19k	3.84 ± 0.13	53.76 ± 2.65	65.43 ± 2.32
CA-4	2.01 ± 0.08	73.58 ± 2.44	83.66 ± 3.12

[a]All data are presented as the mean ± SD from three independent experiments.

[b]Tubulin, 1 μM; [^{3}H]-colchicine, 5 μM; test compounds, 1 or 5 μM.

2.4 Inhibition of Intracellular HDACs and Microtubules

To profile the intracellular inhibition abilities of these dual-target compounds against both the HDACs and microtubules, the representative compound **II-19k** was tested in K562 cells. As shown in Figure 5A, **II-19k** significantly increased the intracellular levels of HDAC6 substrate acetyl-α-tubulin and HDAC1/2/3 substrate acetyl-histone H3, suggesting that **II-19k** could inhibit histone deacetylation in K562 cells. Then compound **II-19k** was further evaluated the inhibitory effects on microtubule organization though immunofluorescent staining assay in K562 cells. Results in Figure 5B showed that K562 cells in control group displayed an intact microtubule network. However, cells treated with **II-19k** at various concentrations

showed disrupted microtubule networks and incomplete cellular architecture. Taken together, these intracellular assays provided strong evidence that **II-19k** could inhibited HDACs and microtubules at the cellular level.
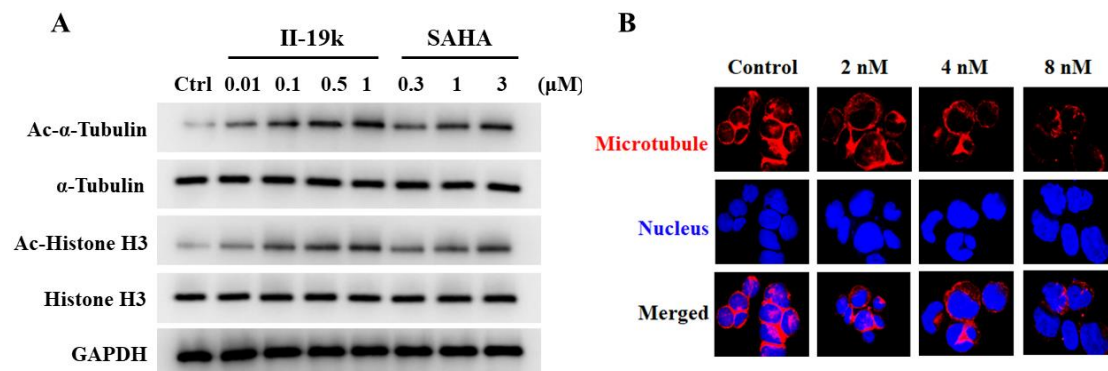

Figure 5. The intracellular inhibition effects of **II-19k** against HDACs and microtubules in K562 cells. (A) Western blot assay was performed to measure levels of acetylated α-tubulin and acetylated histone H3. (B) Immunofluorescence assay was conducted to examine the microtubule network in K562 cells.

2.5 Cell Cycle Analysis

Most of HDAC inhibitors and microtubule polymerization inhibitors can induce cell cycle arrest [31, 32]. In view of this, we used flow cytometry to examine the arrest effects of **II-19k** on K562 cell cycle. As illustrated in Figure 6, treatment of **II-19k** at concentrations of 2, 4, and 8 nM caused a rise of cells in G2 population from 15.36% (control) to 20.48%, 23.38%, and 27.87%, respectively, indicating that **II-19k** arrested K562 cell cycle at the G2 phase. The effects of **II-19k** on the expression of cell cycle regulatory proteins were further tested by Western blotting assay. As shown in Figure 7, compound **II-19k** decreased the expression levels of Cdc2, Cdc25c and Cyclin B1 in a concentration-dependent manner, suggesting that the **II-19k**-induced G2 arrest may be correlated with these regulation proteins.
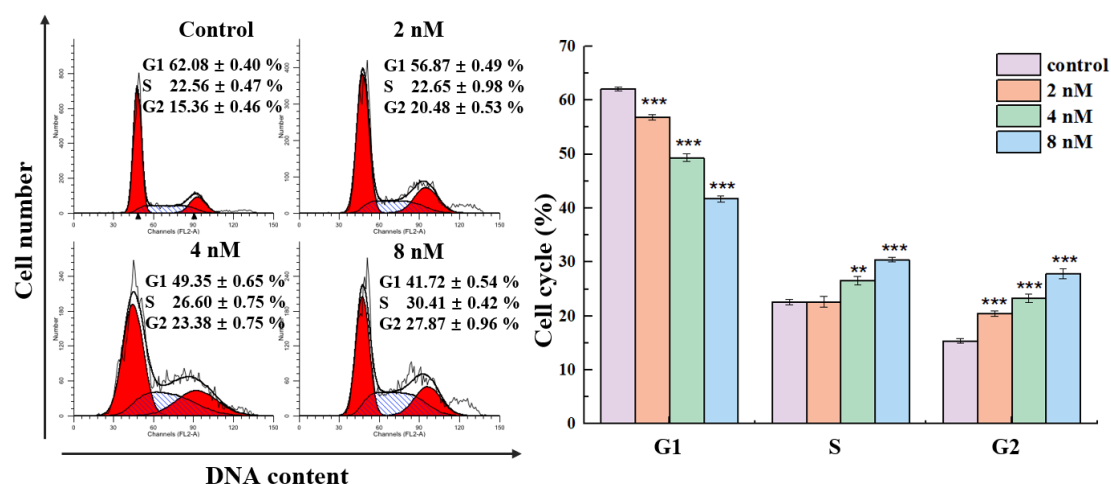
Figure 6. Treatment of K562 cells with compound **II-19k** resulted in induction of G2 phase cell cycle arrest. The cells were stained with propidiumiodide and analyzed via flow cytometry to measure the cell cycle profile. The percentage of cell cycle distribution was presented in the form of histograms. $**p < 0.01$, $***p < 0.001$ *vs.* control group.
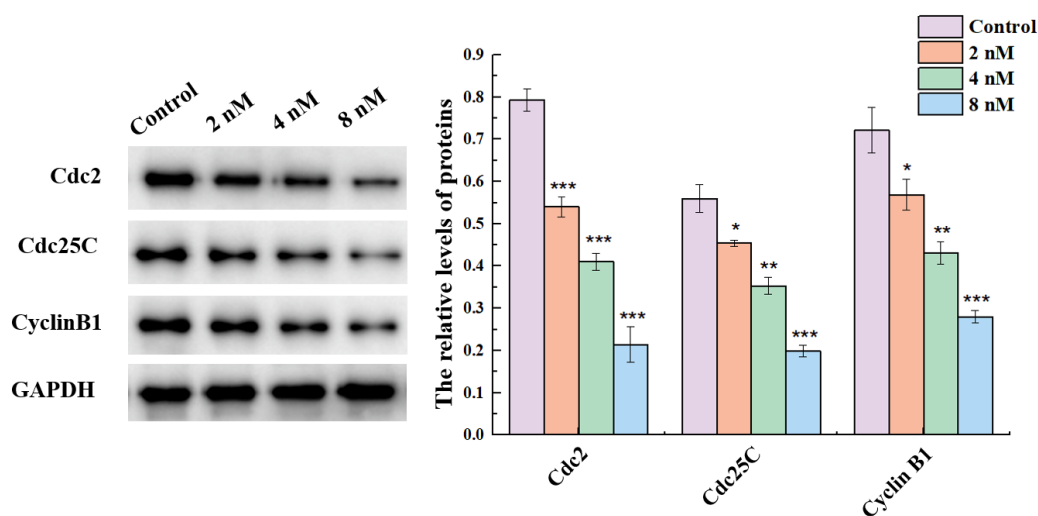

Figure 7. Western blotting assay of cell cycle regulatory proteins. The density ratios of cell cycle regulatory proteins to GADPH were presented in the form of histograms.. $*p < 0.05$, $**p < 0.01$, $***p < 0.001$ *vs.* control group.

2.6 Cell Apoptosis Assay

We further employed Hoechst 33342 staining to observe the changes in morphology

of K562 cells after incubation with varying concentrations of compound **II-19k**. Results displayed in Figure 8A revealed evident morphological changes indicating apoptosis, including chromatin aggregation and nuclear fragmentation. The annexin-V/PI assay also validated the dose-dependent induction of apoptosis by **II-19k** in K562 cells, with cells incubated with 2/4/8 nM showing a rise in apoptotic cells from 18.46% to 43.70% compared to control cells displaying only 4.92% apoptotic cells (Figure 8B). Moreover, Western blot analysis demonstrated that **II-19k** exhibited concentration-dependent pro-apoptotic effects, upregulating the expression of Bad and Bax and downregulating the expression of Bcl-2 and Bcl-xL, as shown in Figure 9.
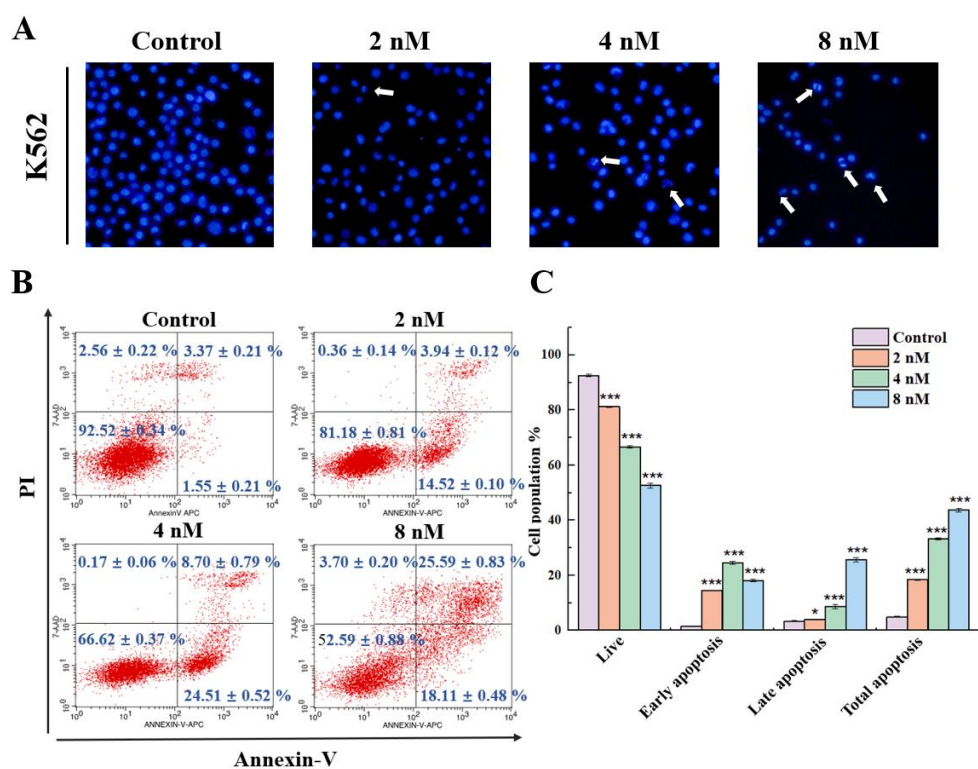

Figure 8. Compound **II-19k** induced apoptosis in K562 cells. (A) Cell morphology and nuclear changes (indicated by white arrows) were observed following incubation with varying concentrations of **II-19k**. (B) Annexin-V/PI staining and flow cytometric analysis. (C) The percentage of cell distribution was presented in the form of histograms. $*p < 0.05$, $***p < 0.001$ *vs*. control group.
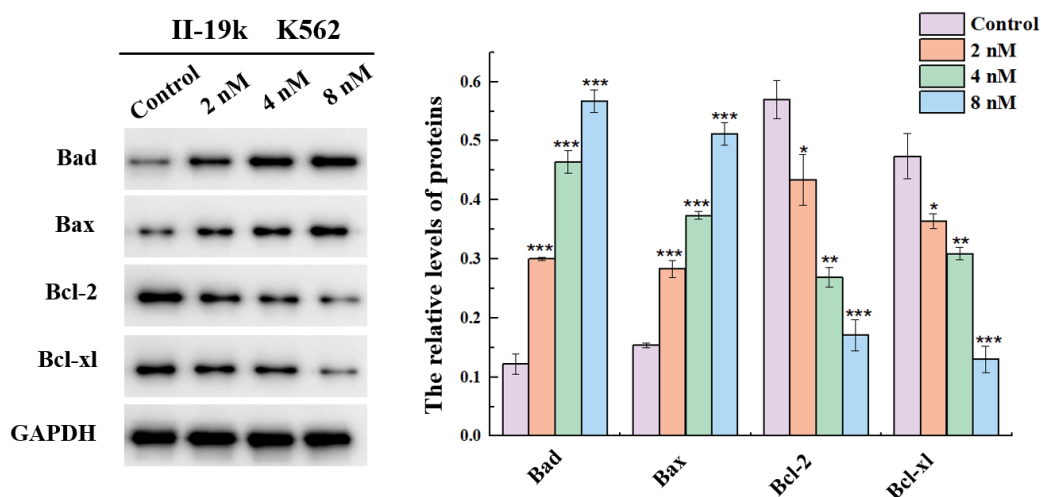
Figure 9. The apoptosis-related protein analysis was conducted via Western blot. The ratios of apoptosis-related proteins to GADPH were presented in the form of histograms. *$p < 0.05$, **$p < 0.01$, ***$p < 0.001$ *vs.* control group.

2.7 In Vitro Evaluation of Mitochondrial Membrane Potential and Reactive Oxygen Species (ROS) Generation

During early apoptosis, mitochondrial membrane permeability increases, resulting in decreased transmembrane potential [33]. To evaluate the impact of compound **II-19k** on K562 cell mitochondrial membrane potential (MMP), we used the JC-1 dyeing assay. At concentrations between 0 and 8 nM, **II-19k** significantly reduced MMP, resulting in a decline of red fluorescence intensity from 93.36% to 57.69%, while green fluorescence intensity increased from 6.63% to 42.31% (Figure 10). Based on these findings, we can conclude that during apoptosis, **II-19k** caused mitochondrial dysfunction in K562 cells by decreasing MMP.

The rise of reactive oxygen species (ROS) is known to promote tumor cell apoptosis by depolarizing the mitochondrial membrane potential [34]. Thus, we detected the intracellular ROS of K562 cells by fluorescent probe DCF-DA (Figure 11). When K562 cells were co-incubated with compound **II-19k**, the proportion of DCF positive cells increased dose-dependently. At higher concentrations of the compound, the proportion of DCF positive cells increased significantly, from 3.87% to 42.67%. These findings suggested that **II-19k** is capable of increasing ROS levels in tumor cells, thereby
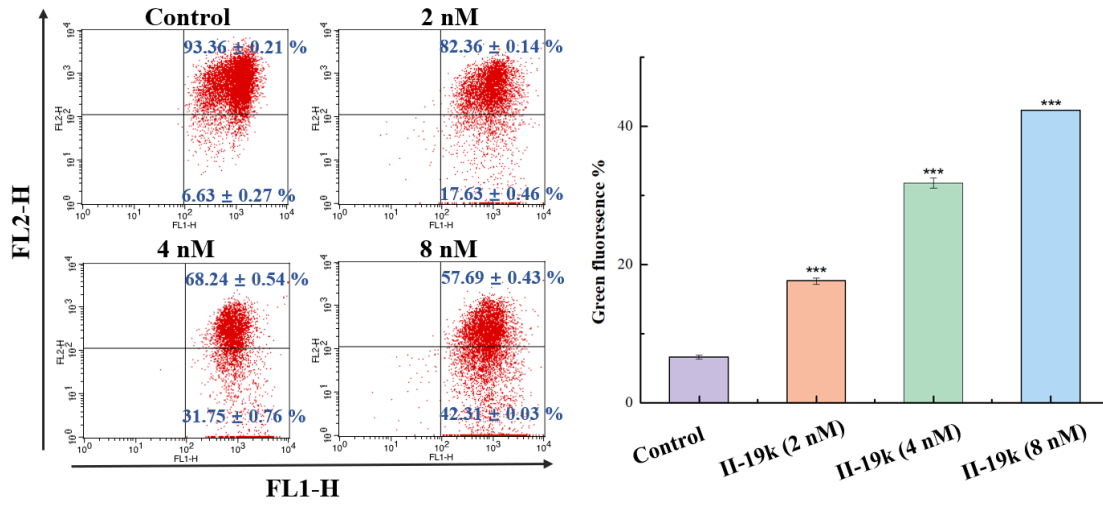
inducing cell death.

Figure 10. Assessment of the MMP via JC-1 dyeing assay. The FACScan flow cytometry was presented in the form of histograms. ***$p < 0.001$ *vs*. control group.
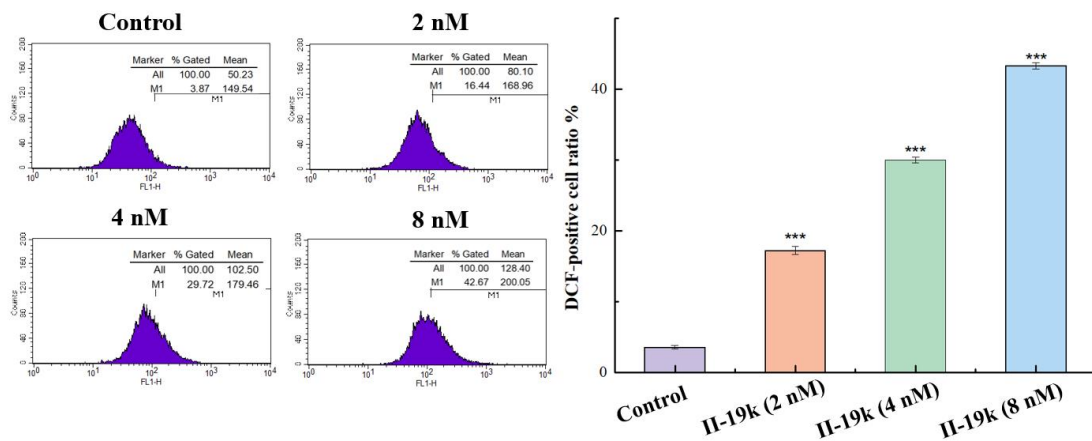

Figure 11. The assessment of ROS generation via DCF-DA and FACScan flow cytometry. The intracellular ROS contents were presented in the form of histograms. ***$p < 0.001$ *vs*. control group.

2.8 In Vitro Inhibition of Migration and Invasion

Tumor cell migration and invasion are directly associated with the process of metastasis in solid tumors [35]. We selected the highly invasive and aggressive MDA-MB-231 cell line for transwell assay to evaluate the inhibitory ability of compound **II-19k** on tumor cell migration and invasion. For the migration assay, MDA-MB-231 cells

were seeded on chambers and incubated with **II-19k** (0, 2, 4, and 8 nM) for 48 h. Cells that migrated through the chambers were stained with crystal violet. As shown in Figure 12, there was a gradual decrease in the number of violet cells as the compound **II-19k** concentration increases, which indicated **II-19k** dose-dependently inhibited MDA-MB-231 cell migration. The similar phenomenon could also be observed in the experiment using Matrigel coated invasion chambers, which revealed that **II-19k** was considerably effective in inhibiting tumor cell invasion. Taken together, these results demonstrated that dual-target stilbene-based inhibitor **II-19k** could effectively inhibit the migration of solid tumors.
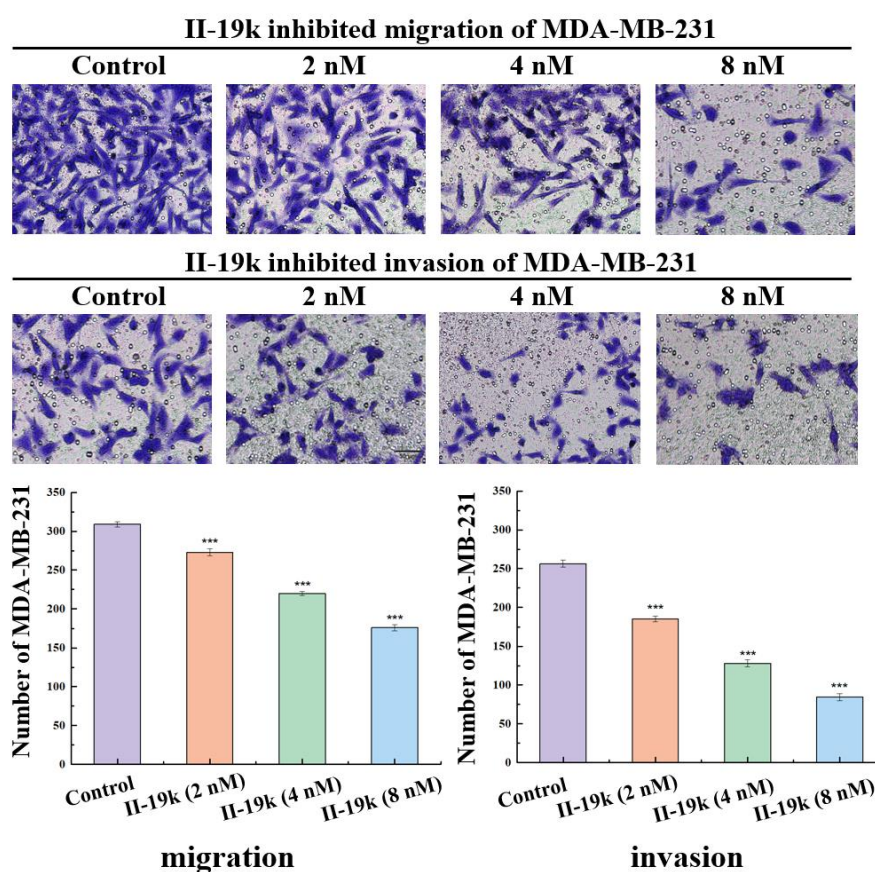

Figure 12. Effects of compound **II-19k** on migration and invasion of MDA-MB-231 cells by transwell assays. The number of migrating cells was presented in the form of histograms. ***$p < 0.001$ *vs*. control group.

2.9 In Vitro Evaluation of Anti-vascular Activity

Angiogenesis is the fundamental of solid tumor growth, which provides necessary

nutrients and oxygen for tumor cell proliferation and metastasis [36]. The wound healing assays were first performed to evaluate whether the dual-target compound **II-19k** could possess vascular disrupting activity. As shown in Figure 13A, HUVECs in the control group were able to migrate to fill the wound channel after 24 h. While compound **II-19k** could potently suppress the migration of HUVECs at the dose of 8 nM, which was even better than the structurally similar parent compound **8**, HDAC inhibitor SAHA and the combination of SAHA + compound **8**. We next evaluated the anti-vascular activity of **II-19k** in a tube formation assay. As shown in Figure 13B, HUVECs in the control group could form tubular and cord-like networks on Matrigel. The capillary-like tubes of HUVECs exposed to **II-19k** at doses of 2, 4 and 8 nM for 6 h could be interrupted at different levels. Among them, the cells treated with **II-19k** at the dose of 8 nM were spherical and aggregated into small clumps, and the suppressing effect was stronger than those of SAHA, compound **8** and the combination. In addition, the IC_{50} value of **II-19k** against HUVECs after a 24 h treatment was 0.192 ± 0.031 μM, which was much higher than the concentration of 8 nM required for the obvious inhibition of cell migration and tube formation. This result indicated that the anti-vascular potential of **II-19k** was not due to the toxicity or cell apoptosis.
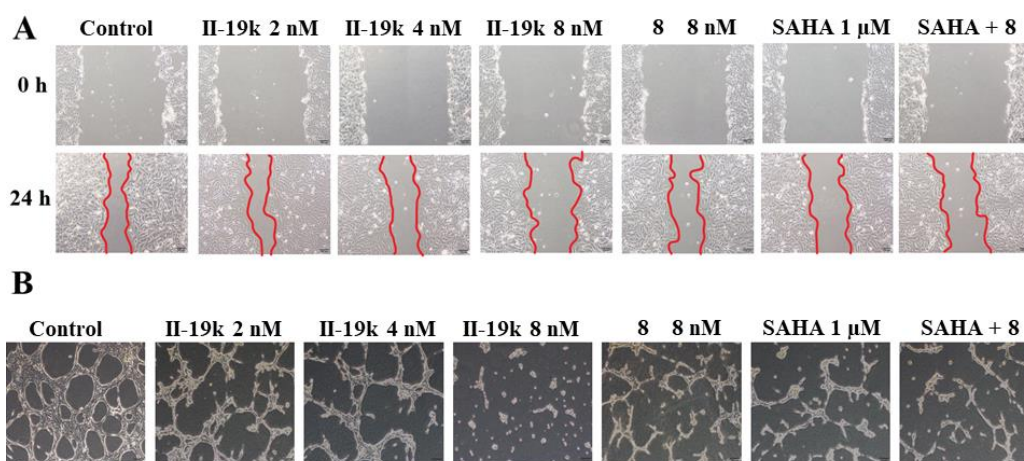

Figure 13. Effects of compound **II-19k** on the HUVECs migration and tube formation. The combination group contained 1 μM SAHA and 8 nM compound **8**. (A) The images of scratch at 0 h and 24 h. (B) The images of HUVEC tubular network formation.

2.10 In Vivo Antitumor Assay

Based on these promising *in vitro* activities, the *in vivo* anti-solid tumor potency of compound **II-19k** was further evaluated in a mouse H22 liver cancer allograft model. Firstly, we conducted an antiproliferation activity test of compound **II-19k** on tumor cells H22 and found that it also exhibited excellent inhibitory activity with an IC_{50} value of 0.008 μM. Then, the *in vivo* antitumor efficacy was investigated. Results in Figure 14 showed that compound **II-19k** had excellent antitumor efficacy with 73.12% tumor growth inhibition (TGI) value (20 mg/kg daily), in which group both the tumor volumes and weights were significantly decreased compared to the structurally similar parent compound **8** (64.07% TGI at a dose of 20 mg/kg daily) and HDAC inhibitor SAHA (57.80% TGI at a dose of 25 mg/kg daily). Moreover, in the **II-19k** treated group, there was no significant decrease in body weight (Figure 14C) or any observable toxic signs in vital organs (Figure 15A), indicating a favorable *in vivo* safety profile of the compound **II-19k**. Additionally, the effects of **II-19k** on tumor microvessels were examined by means of immunohistochemical staining (Figure 15B). The group treated with 20 mg/kg of **II-19k** displayed a considerably lower microvessel density compared to the control group and the parent compound **8** group. These findings provide further evidence of the superior anti-solid tumor efficacy of dual-target inhibition of tubulin and HDACs.
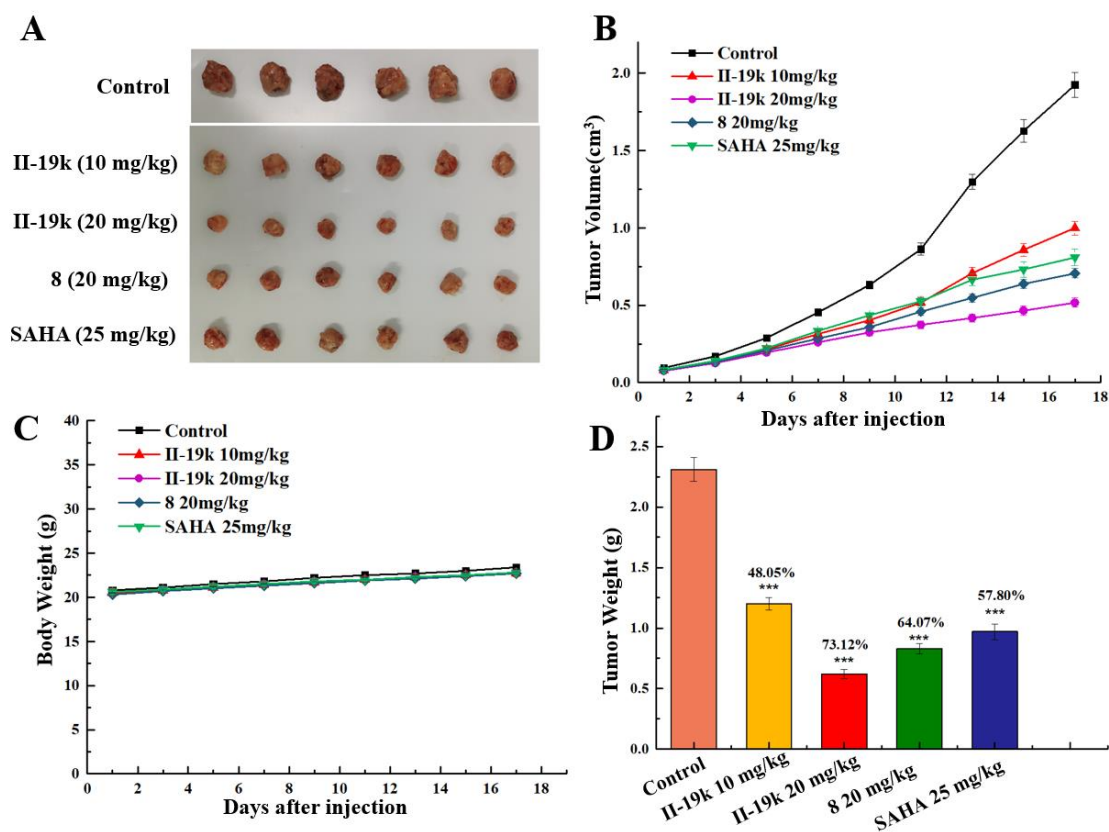
Figure 14. The *in vivo* antitumor efficacy of **II-19k**. Mice bearing H22 allograft tumor were treated with vehicle, compound **8** (20 mg/kg daily, i.v.), compound **II-19k** (10/20 mg/kg daily, i.v.), and SAHA (25 mg/kg daily, i.p.). (A) The image of tumors at the terminal treatment; (B) The changes of tumor volume; (C) The changes of body weight; (D) The weight of the excised tumors from each group. ***p < 0.001 *vs*. control group.

Figure 15. (A) H&E staining of vital organs. (B) Tumor microvessel density via CD31

immunohistochemical staining. ***$p < 0.001$ *vs*. control group.

3. Conclusions

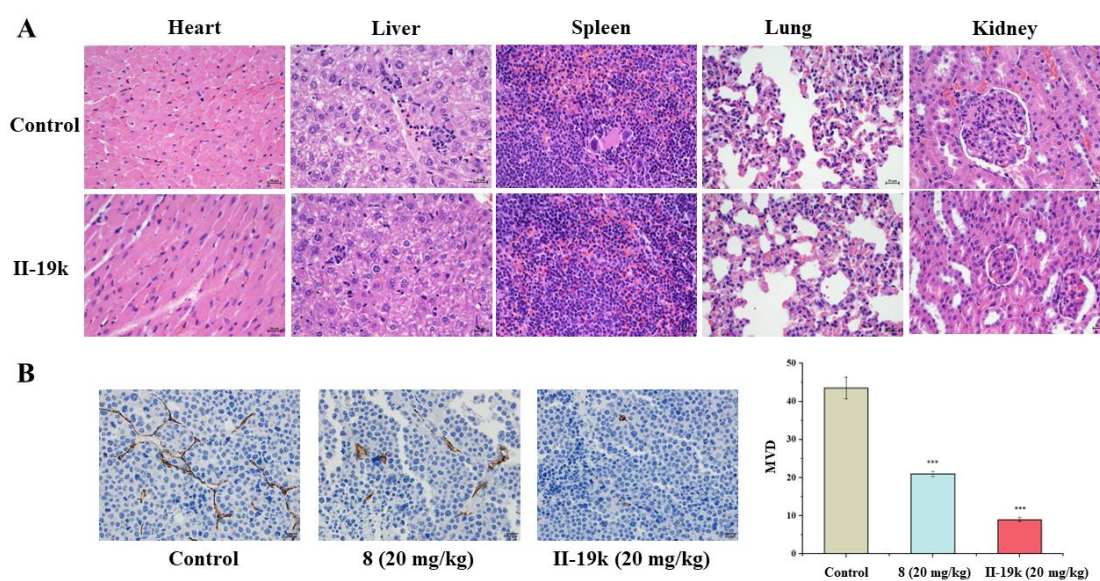In summary, a series of novel stilbene-based derivatives have been designed, synthesized, and evaluated as tubulin/HDAC dual-target inhibitors. The representative compound **II-19k** showed satisfactory antiproliferative activities against both hematological malignancies and solid tumor cell lines with IC$_{50}$ values ranging from 0.003 to 0.036 μM. The mechanism studies demonstrated that **II-19k** could inhibit microtubules and HDACs at the cytological level, and cause tumor cell cycle arrest at G2 phase. Compound **II-19k** also depolarized the mitochondria membrane potentials and generated ROS to induce apoptosis in tumor cells. The transwell assays indicated **II-19k** exerted significant antimetastatic effects on solid tumor cells. The *in vitro* wound healing and tube formation assays of HUVECs showed that the vascular disrupting effects of compound **II-19k** were more pronounced than the combined administration of parent compound **8** and HDAC inhibitor SAHA. Additionally, the antitumor properties of **II-19k** were validated in a mouse liver cancer allograft model without evident toxicity. Compound **II-19k** inhibited the tumor growth and reduced tumor weight by 73.12% at a dose of 20 mg/kg daily (i.v.) compared to the control group, which showed the superiority of dual-target inhibition of tubulin and HDAC. The anti-vascular activity of **II-19k** was further confirmed in the *in vivo* microvascularization of solid tumor tissues. Altogether, these bioactivity results indicated that the optimal compound **II-19k**, as a novel stilbene-based tubulin/HDAC hybrid inhibitor, is a promising lead compound for further development of new antitumor and antiangiogenic agents.

4. Experimental
4.1 Chemistry
4.1.1. General

Most chemical reagents and solvents were obtained from commercial sources. Further purification and drying were performed by standard methods when necessary.

Reactions were monitored by thin-layer chromatography (TLC) on 0.25 mm silica gel plates and visualized though UV light. ^{1}H NMR and ^{13}C NMR spectra were recorded with 300/400/500/600 MHz instruments in the indicated deuterated solvent. The values of the chemical shifts are quoted in δ values (ppm) and the coupling constants (J) in Hz. The low- and high- resolution mass spectra (LRMS and HRMS) were recorded using Finnigan MAT 95 spectrometer.

*4.1.2. General procedure for the preparation of intermediates **S4a~i**.*

To a solution of 4-methylbenzenesulfonhydrazide (60.19 mmol, 2.0 equiv) in anhydrous ethanol (100 mL), acetophenone with different substitution **S1a-e** (30.09 mmol, 1.0 equiv) was added, and the reaction was stirred for 3 h at 85 °C. Upon completion, the resultant mixture was filtered to obtain a white solid, then washed with cold ethanol and dried to afford intermediate **S2a~i**, which was used in the next step without further purification. To a mixture of **S2a~i** (5.03 mmol, 1.3 equiv) and various substituted pyridines or quinolines **S3a~e** (3.87 mmol, 1.0 equiv) in 1,4-dioxane, PdCl$_2$(CH$_3$CN)$_2$ (0.39 mmol, 0.1 equiv), Xphos (0.39 mmol, 0.1 equiv) and *t*-BuOLi (8.51 mmol, 2.2 equiv) were added. The reaction was stirred at 100 °C for 2 h-10 h in a sealed tube. Afterward, the mixture was cooled to room temperature, filtered to remove solid residue. The filtrate was concentrated *in vacuo* and purified by chromatography on silica gel (petroleum ether/ethyl acetate = 20:1) to afford intermediate **S4a~i**.

*4-(1-(3-((tert-butyldimethylsilyl)oxy)-4-methoxyphenyl)vinyl)-2-methylquinoline (**S4a**)*. Yellow oil, yield 73%. ^{1}H NMR (400 MHz, DMSO-d_6) δ 7.95 (dt, J = 8.4, 0.9 Hz, 1H), 7.65 (ddd, J = 8.4, 6.8, 1.4 Hz, 1H), 7.55 (dd, J = 8.3, 1.4 Hz, 1H), 7.37 (ddd, J = 8.3, 6.9, 1.3 Hz, 1H), 7.32 (s, 1H), 6.97 – 6.85 (m, 2H), 6.61 (d, J = 2.1 Hz, 1H), 5.97 (d, J = 0.9 Hz, 1H), 5.31 (d, J = 0.8 Hz, 1H), 3.74 (s, 3H), 2.69 (s, 3H), 0.82 (s, 9H), 0.04 (s, 6H). ESI-MS *m/z* 406.2 [M + H]$^+$.

*4-(1-(4-methoxyphenyl)vinyl)-2-methylquinoline (**S4b**)*. Yellow oil, yield 60%. ^{1}H NMR (300 MHz, DMSO-d_6) δ 8.03 – 7.87 (m, 1H), 7.64 (ddd, J = 8.4, 6.8, 1.4 Hz, 1H), 7.56 (dd, J = 8.4, 1.3 Hz, 1H), 7.35 (ddd, J = 8.2, 6.6, 1.2 Hz, 1H), 7.29 (s, 1H), 7.18 (d, J = 8.8 Hz, 2H), 6.85 (d, J = 8.8 Hz, 2H), 5.97 (s, 1H), 5.27 (s, 1H), 3.70 (s, 3H),

2.67 (s, 3H). ESI-MS *m/z* 276.1 [M + H]$^+$.

4-(1-(3-bromo-4-methoxyphenyl)vinyl)-2-methylquinoline (S4c). Yellow oil, yield 57%. ^{1}H NMR (300 MHz, Chloroform-*d*) δ 8.06 (d, *J* = 8.4 Hz, 1H), 7.72 − 7.60 (m, 2H), 7.58 (d, *J* = 2.2 Hz, 1H), 7.35 (ddd, *J* = 8.3, 7.0, 1.2 Hz, 1H), 7.21 (s, 1H), 7.06 (dd, *J* = 8.6, 2.2 Hz, 1H), 6.77 (d, *J* = 8.7 Hz, 1H), 5.91 (d, *J* = 0.9 Hz, 1H), 5.34 (d, *J* = 0.8 Hz, 1H), 3.87 (s, 3H), 2.78 (s, 3H). ESI-MS *m/z* 354.0 [M + H]$^+$.

methyl 2-methoxy-5-(1-(2-methylquinolin-4-yl)vinyl)benzoate (S4d). Yellow oil, yield 49%. ^{1}H NMR (300 MHz, DMSO-*d*$_6$) δ 7.95 (d, *J* = 8.4 Hz, 1H), 7.66 (dd, *J* = 8.4, 6.7 Hz, 1H), 7.60 − 7.49 (m, 2H), 7.39 (dd, *J* = 7.9, 5.9 Hz, 2H), 7.34 (s, 1H), 7.09 (d, *J* = 8.9 Hz, 1H), 6.04 (s, 1H), 5.37 (s, 1H), 3.79 (s, 3H), 3.71 (s, 3H), 2.68 (s, 3H). ESI-MS *m/z* 334.1 [M + H]$^+$.

4-(1-(3-((tert-butyldimethylsilyl)oxy)phenyl)vinyl)-2-methylquinoline **(S4e)**. Yellow oil, yield 86%. ^{1}H NMR (400 MHz, Chloroform-*d*) δ 8.04 (dt, *J* = 8.4, 0.9 Hz, 1H), 7.69 (ddd, *J* = 8.4, 1.5, 0.6 Hz, 1H), 7.62 (ddd, *J* = 8.4, 6.9, 1.5 Hz, 1H), 7.32 (ddd, *J* = 8.2, 6.9, 1.2 Hz, 1H), 7.22 (s, 1H), 7.14 (t, *J* = 7.9 Hz, 1H), 6.90 − 6.85 (m, 1H), 6.79 − 6.68 (m, 2H), 5.98 (d, *J* = 1.1 Hz, 1H), 5.40 (d, *J* = 1.1 Hz, 1H), 2.77 (s, 3H), 0.90 (s, 9H), 0.06 (s, 6H). ESI-MS *m/z* 376.2 [M + H]$^+$.

4-(1-(3-((tert-butyldimethylsilyl)oxy)-4-methoxyphenyl)vinyl)quinoline **(S4f)**. Yellow oil, yield 60%. ^{1}H NMR (300 MHz, Chloroform-*d*) δ 8.92 (d, *J* = 4.4 Hz, 1H), 8.21 − 8.02 (m, 1H), 7.75 (dd, *J* = 8.5, 1.3 Hz, 1H), 7.66 (ddd, *J* = 8.4, 6.8, 1.4 Hz, 1H), 7.46 − 7.37 (m, 1H), 7.33 (d, *J* = 4.3 Hz, 1H), 6.81 (d, *J* = 2.0 Hz, 1H), 6.76 − 6.71 (m, 2H), 5.89 (d, *J* = 1.1 Hz, 1H), 5.30 (d, *J* = 1.0 Hz, 1H), 3.78 (s, 3H), 0.91 (s, 9H), 0.04 (s, 6H). ESI-MS *m/z* 392.2 [M + H]$^+$.

4-(1-(3-((tert-butyldimethylsilyl)oxy)-4-methoxyphenyl)vinyl)-2-methylpyridine **(S4g)**. Yellow oil, yield 86%. ^{1}H NMR (300 MHz, Chloroform-*d*) δ 8.44 (d, *J* = 5.2 Hz, 1H), 7.09 (s, 1H), 7.05 (dd, *J* = 5.3, 1.6 Hz, 1H), 6.88 − 6.80 (m, 2H), 6.78 (d, *J* = 2.2 Hz, 1H), 5.46 (d, *J* = 11.6 Hz, 2H), 3.82 (s, 3H), 2.54 (s, 3H), 0.97 (s, 9H), 0.14 (s, 6H). ESI-MS *m/z* 356.2 [M + H]$^+$.

4-(1-(3-((tert-butyldimethylsilyl)oxy)-4-methoxyphenyl)vinyl)-2-methoxypyridine **(S4h)**. Yellow oil, yield 88%. ^{1}H NMR (300 MHz, Chloroform-*d*) δ 8.30 (t, *J* = 7.1 Hz,

1H), 7.01 (d, $J = 3.8$ Hz, 1H), 6.78 (d, $J = 6.5$ Hz, 2H), 6.60 (s, 2H), 5.70 (d, $J = 5.8$ Hz, 1H), 5.41 (d, $J = 5.8$ Hz, 1H), 3.95 (s, 3H), 3.85 (s, 3H), 1.00 (s, 9H), 0.14 (s, 6H). ESI-MS *m/z* 372.2 [M + H]+.

4-(1-(3-((tert-butyldimethylsilyl)oxy)-4-methoxyphenyl)vinyl)-2,6-dimethylpyridine (S4i). Yellow oil, yield 66%. ^{1}H NMR (300 MHz, Chloroform-*d*) δ 6.91 (s, 2H), 6.84 (d, $J = 2.0$ Hz, 1H), 6.82 (s, 1H), 6.78 (d, $J = 2.1$ Hz, 1H), 5.45 (dd, $J = 11.6, 1.1$ Hz, 2H), 3.83 (s, 3H), 2.51 (s, 6H), 0.97 (s, 9H), 0.14 (s, 6H). ESI-MS *m/z* 370.2 [M + H]+.

4.1.3. Synthesis of (E)-3-(4-(1-(1H-indol-5-yl)vinyl)quinolin-2-yl)-N-hydroxyacrylamide (I-12a)

To the solution of 1-(1*H*-indol-5-yl)ethan-1-one (**S5**, 500 mg, 3.14 mmol) in anhydrous THF (20 mL), NaH (188 mg, 4.71 mmol) was added. The mixture was stirred at 0 °C for 30 min and subsequently (Boc)$_2$O (822 mg, 4.71 mmol) dissolved in THF (5 mL) was added dropwise. After addition was completed, the resulting mixture was stirred at room temperature for 20 min. Afterward, the mixture was diluted by water, and extracted with ethyl acetate (3 × 50 mL). The combined organic layers were washed with brine, dried over anhydrous Na$_2$SO$_4$, and concentrated *in vacuo* to provide intermediate **S6**. The compounds **S8** was prepared by the similar procedure of intermediate **S4a~i** from intermediate **S6**. To a solution of **S8** (718 mg, 1.87 mmol) in 25 mL of 1,4-dioxane, SeO$_2$ (249 mg, 2.24 mmol) was added. The reaction was stirred at 100 °C for 20 min and quenched with water (5 mL). The residue was extracted with ethyl acetate (3 × 30 mL). The combined organic layers were washed with brine, dried over anhydrous Na$_2$SO$_4$, and concentrated *in vacuo* to provide intermediate **S9**. To a solution of NaH (15 mg, 361.39 μmol) in anhydrous THF (10 mL), ethyl 2-(diethoxyphosphoryl)acetate (72 μL, 361.39 μmol) was added at 0 °C under Ar. The solution was stirred for 30 min at 0 °C. The solution of intermediate **S9** (120 mg, 301.16 μmol) was then added dropwise and stirred for another 1 h at 70 °C. Upon reaction completion, the reaction was diluted by water, and extracted with ethyl acetate (3 × 10 mL). The combined organic layers were washed with brine, dried over anhydrous Na$_2$SO$_4$, and concentrated *in vacuo* to provide intermediate **S10a**. To a solution of

intermediate **S10a** (200 mg, 426.85 μmol) in dichloromethane (5 mL), 0.5 mL acetic acid was added. The reaction was stirred at room temperature for 2 h. Upon reaction completion, the solvent was removed *in vacuo*, then the residue was dissolved into saturated sodium bicarbonate solution (20 mL), and extracted with ethyl acetate (3 × 20 mL). The combined organic layers were washed with brine, dried over anhydrous Na_2SO_4, and concentrated *in vacuo* to provide ester intermediate **S11a**. **S11a** was dissolved in fresh hydroxylamine hydrochloride solution, and the mixtures were stirred at room temperature for 20 min. Upon reaction completion, the solvent was removed *in vacuo*, then the residue was dissolved into water, and followed by neutralization with 2 N HCl aqueous. The resulting precipitate was collected by filtration, washed by water, and dried to afford crude products. Finally, these crude products were purified by flash chromatography on silica gel (dichloromethane/methanol = 30:1) to give target compound **I-12a**. White solid, yield 60%. ^{1}H NMR (300 MHz, DMSO-d_6) δ 11.38 (s, 1H), 11.16 (s, 1H), 8.02 (d, J = 8.4 Hz, 1H), 7.70 (s, 2H), 7.66 (dd, J = 8.5, 4.9 Hz, 2H), 7.41 (t, J = 7.6 Hz, 1H), 7.36 (s, 1H), 7.31 (s, 3H), 7.21 − 7.09 (m, 2H), 6.33 (s, 1H), 6.03 (s, 1H), 5.32 (s, 1H). ^{13}C NMR (75 MHz, DMSO-d_6) δ 153.9, 150.2, 148.3, 147.0, 138.4, 136.2, 130.9, 130.4, 129.9, 128.1, 127.3, 126.9, 126.7, 126.4, 125.3, 121.8, 120.0, 118.9, 115.4, 112.1, 102.1. HR-MS (ESI) *m/z*: calcd for $C_{22}H_{18}N_3O_2$ [M + H]$^+$ 356.1394 found 356.1399.

4.1.4. Synthesis of 4-(1-(1H-indol-5-yl)vinyl)-N-(2-aminophenyl)quinoline-2-carboxamide (I-12b)

To a solution of intermediate **S9** (150 mg, 376.45 μmol) and 2-methyl-2-butene (316 μL, 3.76 mmol) in *tert*-butanol (5 mL), sodium chlorite (85 mg, 941.12 μmol) and sodium dihydrogen phosphate (90 mg, 752.89 μmol) dissolved in 2mL water were added. The reaction was stirred at room temperature for 4 h. Upon reaction completion, the resulting precipitate was collected by filtration to afford intermediate **S10b**. To a solution of **S10b** (60 mg, 144.77 μmol) and benzene-1,2-diamine (16 mg, 144.77 μmol) in anhydrous DMF, EDCI (33 mg, 173.72 μmol), HOBT (23 mg, 173.72 μmol) and DIPEA (63 μL, 361.92 μmol) were added. The reaction was stirred overnight at room temperature. Then, the mixtures were diluted with water and extracted with ethyl

acetate (3 × 20 mL). The combined organic layers were washed with brine, dried over anhydrous Na_2SO_4, and concentrated *in vacuo* to provide intermediate **S11b**, which was dissolved in a solution of DCM/ CH_3COOH (3/1) to remove the Boc protective group and subsequently purified by column chromatography (PE/EA=1/1) to afford target compound **I-12b**. Yellow solid, yield 43%. ^1H NMR (300 MHz, DMSO-d_6) δ 11.19 (s, 1H), 10.25 (s, 1H), 8.26 (s, 1H), 8.10 (s, 1H), 7.81 (dd, J = 8.3, 6.9 Hz, 2H), 7.55 (ddd, J = 16.8, 7.5, 1.3 Hz, 2H), 7.37 – 7.30 (m, 3H), 7.18 (dd, J = 8.6, 1.8 Hz, 1H), 6.99 (td, J = 7.6, 1.5 Hz, 1H), 6.85 (dd, J = 8.0, 1.4 Hz, 1H), 6.67 (td, J = 7.5, 1.5 Hz, 1H), 6.33 (s, 1H), 6.08 (s, 1H), 5.37 (s, 1H), 5.03 (s, 2H).^{13}C NMR (100 MHz, DMSO-d_6) δ 162.9, 151.2, 150.4, 147.0, 146.9, 142.6, 136.2, 131.0, 130.8, 130.4, 128.7, 128.2, 128.0, 126.8, 126.7, 126.5, 125.4, 124.1, 120.1, 119.3, 119.0, 117.4, 117.1, 115.8, 112.2, 102.2. HR-MS (ESI) *m/z*: calcd for $C_{26}H_{21}N_4O$ [M + H]$^+$ 405.1710 found 405.1713.

*4.1.5.   Synthesis   of   2-((4-(1-(1H-indol-5-yl)vinyl)quinolin-2-yl)methoxy)-N-hydroxyacetamide (**I-12c**)*

To a solution of intermediate **S9** (891 mg, 2.24 mmol) in anhydrous THF (25 mL), sodium borohydride (169 mg, 4.47 mmol) was added. The reaction was stirred at room temperature for 30 min and quenched with saturated ammonium chloride solution (10 mL). The residue was extracted with ethyl acetate (3 × 30 mL). The combined organic layers were washed with brine, dried over anhydrous Na_2SO_4, and concentrated *in vacuo* to provide intermediate **S10c**. To a solution of **S10c** (147 mg, 367.06 μmol) in anhydrous THF (25 mL), NaH (177 mg, 44.05 mmol) was added under ice bath. After the reaction was stirred for 30 min, ethyl bromoacetate (204 μL, 1.84 mmol) in THF was then added dropwise. The resultant mixtures were stirred overnight at room temperature. At the end of the reaction, the solvent was concentrated *in vacuo* to afford intermediate **S11c**. **S11c** was then subjected to the above similar procedure to remove the Boc protective group and hydroxylamine to obtain the target compound **I-12c**. Orange solid, yield 56%. ^1H NMR (400 MHz, DMSO-d_6) δ 11.26 (s, 1H), 9.86 (s, 2H), 8.00 (d, J = 8.4 Hz, 1H), 7.77 – 7.60 (m, 3H), 7.38 (dd, J = 15.8, 8.1 Hz, 2H), 7.31 (t, J = 2.4 Hz, 2H), 7.22 – 7.08 (m, 1H), 6.32 (d, J = 2.8 Hz, 1H), 6.01 (s, 1H), 5.29 (s, 1H), 4.85 (s, 2H), 4.08 (s, 2H). ^{13}C NMR (100 MHz, DMSO-d_6) δ 165.8, 158.9, 145.0, 147.6,

147.3, 136.2, 131.0, 130.0, 129.4, 128.1, 126.8, 126.7, 126.4, 120.2, 120.0, 119.5, 118.9, 115.2, 112.1, 102.1, 74.4, 69.6. HR-MS (ESI) *m/z*: calcd for $C_{22}H_{20}N_3O_3$ $[M + H]^+$ 374.1499 found 374.1505.

*4.1.6. Synthesis of (E)-N-hydroxy-3-(4-(1-(3-hydroxy-4-methoxyphenyl)vinyl)quinolin-2-yl)acrylamide (**I-12d**)*

Following the similar procedure described for preparation of compound **I-12a**. Yellow solid, yield 88%. ^{1}H NMR (300 MHz, DMSO-*d*6) *δ* 10.59 (s, 1H), 9.07 (s, 2H), 8.00 (dd, *J* = 18.0, 8.4 Hz, 1H), 7.78 – 7.67 (m, 1H), 7.65 (d, *J* = 5.2 Hz, 1H), 7.62 – 7.53 (m, 1H), 7.53 – 7.45 (m, 1H), 7.46 – 7.31 (m, 1H), 7.14 (d, *J* = 15.6 Hz, 1H), 6.83 (dd, *J* = 8.4, 5.1 Hz, 1H), 6.73 (dd, *J* = 5.9, 2.2 Hz, 1H), 6.64 (ddd, *J* = 10.6, 8.4, 2.2 Hz, 1H), 5.92 (d, *J* = 14.5 Hz, 1H), 5.27 (d, *J* = 15.3 Hz, 1H), 3.73 (s, 3H). ^{13}C NMR (75 MHz, DMSO-*d*6) *δ* 162.5, 153.8, 149.5, 148.4, 148.3, 148.2, 146.8, 146.7, 145.3, 138.5, 132.5, 130.6, 129.9, 127.5, 126.7, 126.2, 125.2, 121.5, 118.1, 113.8, 56.0. HR-MS (ESI) *m/z*: calcd for $C_{21}H_{19}N_2O_4$ $[M + H]^+$ 363.1339 found 363.1339.

*4.1.7. Synthesis of N-(2-aminophenyl)-4-(1-(3-hydroxy-4-methoxyphenyl)vinyl)quinoline-2-carboxamide (**I-12e**)*

Following the similar procedure described for preparation of compound **I-12b**. Yellow oil, yield 40%. ^{1}H NMR (300 MHz, DMSO-*d*6) *δ* 10.23 (s, 1H), 9.03 (s, 1H), 8.24 (d, *J* = 8.4 Hz, 1H), 8.03 (s, 1H), 7.86 (t, *J* = 7.7 Hz, 1H), 7.77 (d, *J* = 8.1 Hz, 1H), 7.62 (t, *J* = 7.6 Hz, 1H), 7.55 – 7.47 (m, 1H), 7.04 – 6.93 (m, 1H), 6.90 – 6.79 (m, 2H), 6.75 – 6.60 (m, 3H), 5.99 (s, 1H), 5.34 (s, 1H), 5.00 (s, 2H), 3.73 (s, 3H). ^{13}C NMR (75 MHz, DMSO-*d*6) *δ* 162.9, 150.5, 150.4, 148.5, 147.0, 146.8, 145.4, 142.6, 132.6, 131.0, 130.4, 128.8, 127.9, 126.7, 126.4, 125.4, 124.1, 119.3, 118.2, 117.4, 117.1, 116.4, 114.0, 112.6, 56.0. HR-MS (ESI) *m/z*: calcd for $C_{25}H_{21}N_3NaO_3$ $[M + Na]^+$ 434.1475 found 434.1475.

*4.1.8. Synthesis of N-hydroxy-2-((4-(1-(3-hydroxy-4-methoxyphenyl)vinyl)quinolin-2-yl)methoxy)acetamide (**I-12f**)*

Following the similar procedure described for preparation of compound **I-12c**. Yellow oil, yield 66%. ^{1}H NMR (300 MHz, DMSO-*d*6) *δ* 10.88 (s, 1H), 9.00 (s, 2H), 8.00 (d, *J* = 8.3 Hz, 1H), 7.70 (t, *J* = 7.6 Hz, 1H), 7.63 (d, *J* = 8.2 Hz, 1H), 7.58 (s, 1H),

7.45 (t, J = 7.6 Hz, 1H), 6.84 (d, J = 8.3 Hz, 1H), 6.74 – 6.56 (m, 2H), 5.93 (s, 1H), 5.27 (s, 1H), 4.82 (s, 2H), 4.07 (s, 2H), 3.72 (s, 3H). ^{13}C NMR (100 MHz, DMSO-d_6) δ 166.0, 158.8, 149.2, 148.3, 147.6, 146.9, 145.7, 132.6, 130.1, 129.4, 126.9, 126.3, 126.2, 120.2, 118.1, 115.7, 113.9, 112.5, 74.4, 69.5, 56.0. HR-MS (ESI) m/z: calcd for $C_{21}H_{21}N_2O_5$ [M + H]$^+$ 381.1445 found 381.1442.

*4.1.9. Synthesis of (E)-N-hydroxy-3-(4-(1-(4-methoxyphenyl)vinyl)quinolin-2-yl)acrylamide (**I-12g**)*

Following the similar procedure described for preparation of compound **I-12a**. orange solid, yield 78%. ^{1}H NMR (300 MHz, DMSO-d_6) δ 11.00 (s, 1H), 9.38 (d, J = 60.3 Hz, 1H), 8.04 (d, J = 8.4 Hz, 1H), 7.75 (dd, J = 6.8, 1.6 Hz, 1H), 7.73 – 7.66 (m, 2H), 7.66 – 7.62 (m, 1H), 7.52 – 7.43 (m, 1H), 7.26 – 7.19 (m, 2H), 7.14 (d, J = 15.6 Hz, 1H), 6.89 (d, J = 8.7 Hz, 2H), 6.05 (s, 1H), 5.35 (s, 1H), 3.73 (s, 3H). ^{13}C NMR (75 MHz, DMSO-d_6) δ 159.7, 154.0, 149.3, 148.3, 145.1, 132.1, 130.4, 130.0, 128.1, 127.4, 126.6, 126.1, 121.8, 116.1, 114.6, 114.5, 55.6. HR-MS (ESI) m/z: calcd for $C_{21}H_{19}N_2O_3$ [M + H]$^+$ 347.1390 found 347.1390.

*4.1.10. Synthesis of N-(2-aminophenyl)-4-(1-(4-methoxyphenyl)vinyl)quinoline-2-carboxamide (**I-12h**)*

Following the similar procedure described for preparation of compound **I-12b**. Yellow solid, yield 67%. ^{1}H NMR (300 MHz, DMSO-d_6) δ 10.23 (s, 1H), 8.25 (d, J = 8.4 Hz, 1H), 8.04 (d, J = 0.9 Hz, 1H), 7.85 (t, J = 7.6 Hz, 1H), 7.75 (d, J = 8.4 Hz, 1H), 7.61 (t, J = 7.6 Hz, 1H), 7.51 (d, J = 7.8 Hz, 1H), 7.30 – 7.11 (m, 2H), 6.99 (t, J = 7.6 Hz, 1H), 6.87 (dd, J = 12.0, 8.2 Hz, 3H), 6.67 (t, J = 7.5 Hz, 1H), 6.08 (s, 1H), 5.38 (s, 1H), 5.00 (s, 2H), 3.82 – 3.61 (m, 3H). ^{13}C NMR (75 MHz, DMSO-d_6) δ 162.9, 159.8, 150.5, 150.3, 146.9, 145.1, 142.6, 132.1, 131.0, 130.5, 128.8, 128.2, 127.8, 126.7, 126.3, 125.4, 124.1, 119.3, 117.8, 117.4, 117.1, 114.6, 55.6. HR-MS (ESI) m/z: calcd for $C_{25}H_{21}N_3NaO_2$ [M + Na]$^+$ 418.1526 found 418.1526.

*4.1.11. Synthesis of N-hydroxy-2-((4-(1-(4-methoxyphenyl)vinyl)quinolin-2-yl)methoxy)acetamide (**I-12i**)*

Following the similar procedure described for preparation of compound **I-12c**. Yellow solid, yield 80%. ^{1}H NMR (400 MHz, DMSO-d_6) δ 10.91 (s, 1H), 8.95 (s, 1H),

8.01 (d, J = 8.2 Hz, 1H), 7.65 (dt, J = 29.9, 5.7 Hz, 3H), 7.43 (t, J = 7.5 Hz, 1H), 7.28 – 7.10 (m, 2H), 6.96 – 6.78 (m, 2H), 6.01 (s, 1H), 5.30 (s, 1H), 4.84 (s, 2H), 4.08 (s, 2H), 3.70 (s, 3H). ^{13}C NMR (100 MHz, DMSO-d_6) δ 166.0, 159.7, 158.9, 149.1, 147.6, 145.3, 132.2, 130.1, 129.5, 128.1, 126.9, 126.2, 120.2, 115.9, 114.5, 74.4, 69.5, 55.6. HR-MS (ESI) m/z: calcd for $C_{21}H_{21}N_2O_4$ [M + H]$^+$ 365.1496 found 365.1491.

4.1.12. Synthesis of (E)-N-hydroxy-3-(2-methoxy-5-(1-(2-methylquinolin-4-yl)vinyl)phenyl)acrylamide (II-19a)

To a mixture of intermediate **S4c** (70 mg, 197.60 μmol) and methyl acrylate (107 μL, 1.19 mmol) in anhydrous DMF (5 mL), Pd(PPh$_3$)$_2$Cl$_2$ (15 mg, 0.02 mmol) and Et$_3$N (192 μL, 1.38 mmol) were added. The reaction was stirred overnight at 160 °C in a sealed tube under Ar. The reaction was quenched with water (10 mL). The residue was extracted with ethyl acetate (3 × 10 mL). The combined organic layers were washed with brine, dried over anhydrous Na$_2$SO$_4$, and concentrated *in vacuo* to provide intermediate **S18**, which as subjected to the hydroxylamination procedure described above to give the target compound **II-19a**. Yellow solid, yield 30%. ^{1}H NMR (300 MHz, DMSO-d_6) δ 10.68 (s, 1H), 8.98 (s, 1H), 7.95 (d, J = 8.4 Hz, 1H), 7.70 – 7.53 (m, 3H), 7.49 (s, 1H), 7.43 – 7.31 (m, 2H), 7.12 (s, 1H), 7.00 (d, J = 8.5 Hz, 1H), 6.41 (d, J = 16.0 Hz, 1H), 6.05 (s, 1H), 5.35 (s, 1H), 3.83 (d, J = 1.3 Hz, 3H), 2.69 (s, 3H). ^{13}C NMR (150 MHz, DMSO-d_6) δ 159.2, 157.9, 148.1, 147.9, 145.1, 132.7, 132.6, 132.6, 132.5, 129.7, 129.4, 129.2, 126.2, 126.1, 125.9, 125.1, 123.8, 122.7, 120.6, 116.7, 112.4, 56.2. HR-MS (ESI) m/z: calcd for $C_{22}H_{21}N_2O_3$ [M + H]$^+$ 361.1547 found 361.1543.

4.1.13. Synthesis of N-hydroxy-2-methoxy-5-(1-(2-methylquinolin-4-yl)vinyl)benzamide (II-19b)

Intermediate **S4d** as subjected to the hydroxylamination procedure described above to give the target compound **II-19b**. Yellow solid, yield 45%. ^{1}H NMR (300 MHz, DMSO-d_6) δ 10.64 (s, 1H), 9.06 (s, 1H), 7.95 (d, J = 8.4 Hz, 1H), 7.66 (ddd, J = 8.3, 6.6, 1.4 Hz, 1H), 7.56 (d, J = 8.2 Hz, 1H), 7.46 – 7.25 (m, 4H), 7.03 (d, J = 8.7 Hz, 1H), 6.03 (s, 1H), 5.34 (s, 1H), 3.80 (s, 3H), 2.68 (s, 3H). ^{13}C NMR (150 MHz, DMSO-d_6) δ 163.1, 159.2, 157.0, 148.1, 147.9, 144.8, 132.0, 130.0, 129.8, 129.2, 128.0, 126.2, 125.9, 125.1, 123.1, 122.7, 116.7, 112.6, 56.3, 25.3. HR-MS (ESI) m/z: calcd for

$C_{20}H_{18}N_2NaO_3$ $[M + Na]^+$ 357.1210 found 357.1219.

4.1.14. Synthesis of N-(2-aminophenyl)-2-methoxy-5-(1-(2-methylquinolin-4-yl)vinyl)benzamide (II-19c)

To a solution of intermediate **S4d** (80 mg, 239.96 μmol) in THF (25 mL), NaOH (77 mg, 1.92 mmol) was added. The reaction was stirred overnight at 40 °C. Upon reaction completion, the mixtures were diluted with water, and followed by acidification with 2 N HCl aqueous. The residue was extracted with dichloromethane (3 × 30 mL). The combined organic layers were washed with brine, dried over anhydrous Na_2SO_4, and concentrated *in vacuo* to provide carboxylic acid intermediate **S20**. To a solution of **S20** (115 mg, 360.10 μmol) and benzene-1,2-diamine (39 mg, 360.10 μmol) in anhydrous DMF, EDCI (83 mg, 432.11 μmol), HOBT (59 mg, 432.11 μmol) and DIPEA (157 μL, 900.24 μmol) were added. The reaction was stirred at room temperature for 2 h. Then, the mixtures were diluted with saturated sodium bicarbonate solution and extracted with ethyl acetate (3 × 20 mL). The combined organic layers were washed with brine, dried over anhydrous Na_2SO_4, and concentrated *in vacuo*. The residue was purified by column chromatography (PE/EA=1/1) to afford target compound **II-19c**. Yellow solid, yield 78%. ^1H NMR (300 MHz, DMSO-d_6) δ 9.59 (s, 1H), 8.01 (d, J = 8.4 Hz, 1H), 7.81 – 7.57 (m, 3H), 7.50 – 7.41 (m, 3H), 7.39 (s, 1H), 7.19 (d, J = 8.7 Hz, 1H), 7.03 – 6.89 (m, 1H), 6.82 (dd, J = 8.0, 1.4 Hz, 1H), 6.62 (td, J = 7.6, 1.4 Hz, 1H), 6.12 (s, 1H), 5.42 (s, 1H), 4.90 (s, 2H), 3.95 (s, 3H), 2.74 (s, 3H). ^{13}C NMR (75 MHz, DMSO-d_6) δ 163.8, 159.3, 157.3, 148.2, 147.9, 144.9, 141.9, 132.3, 130.6, 129.8, 129.3, 128.5, 126.3, 126.2, 125.9, 125.1, 125.1, 124.5, 124.2, 122.8, 117.1, 116.7, 113.0, 56.7, 55.4, 25.3. HR-MS (ESI) *m/z*: calcd for $C_{26}H_{24}N_3O_2$ $[M + H]^+$ 410.1863 found 410.1863.

*4.1.15. General procedure for the preparation of target compounds **II-19d~v** and **II-25a~l**.*

To a solution of intermediate **S4a**, **e**, **f**, and **S4g~i** (3.19 mmol, 1.0 equiv) in THF, 1 M of TBAF (3.19 mmol, 1.0 equiv) in THF was added dropwise. The reaction was stirred at room temperature for 10 min. Then, the mixtures were diluted with water and extracted with ethyl acetate (3 × 30 mL). The combined organic layers were washed

with brine, dried over anhydrous Na$_2$SO$_4$, and concentrated *in vacuo* to provide hydroxyl intermediate **S21a**, **e**, **f**, and **S23g~i**. To a solution of the hydroxyl intermediate (1.52 mmol, 1.0 equiv), Cs$_2$CO$_3$ (1.67 mmol, 1.1 equiv) and TBAI (0.15 mmol, 0.1 equiv) in acetonitrile, various bromoalkyl ester (2.28 mmol, 1.5 equiv) was added dropwise. The reaction was stirred at 85 °C for 30 min-2 h. Upon reaction completion, the mixtures were diluted with water and extracted with ethyl acetate (3 × 30 mL). The combined organic layers were washed with brine, dried over anhydrous Na$_2$SO$_4$, and concentrated *in vacuo* to provide ester intermediate **S22a~v** and **S24a-l**, which was subjected to the hydroxylamination procedure described above to give the target compound **II-19d~v** and **II-25a~l**.

N-hydroxy-2-(2-methoxy-5-(1-(2-methylquinolin-4-yl)vinyl)phenoxy)acetamide (II-19d). Yellow solid, yield 50%. ^{1}H NMR (300 MHz, DMSO-d_6) δ 10.76 (s, 1H), 9.03 (s, 1H), 7.94 (d, J = 8.4 Hz, 1H), 7.66 (ddd, J = 8.3, 6.8, 1.4 Hz, 1H), 7.58 (d, J = 8.3 Hz, 1H), 7.38 (ddd, J = 8.2, 6.9, 1.3 Hz, 1H), 7.31 (s, 1H), 7.19 (d, J = 2.1 Hz, 1H), 6.84 (d, J = 8.4 Hz, 1H), 6.48 (dd, J = 8.4, 2.0 Hz, 1H), 5.99 (s, 1H), 5.31 (s, 1H), 4.44 (s, 2H), 3.73 (s, 3H), 2.68 (s, 3H). ^{13}C NMR (75 MHz, DMSO-d_6) δ 164.9, 159.1, 149.9, 148.2, 148.1, 147.9, 145.3, 132.4, 129.7, 129.1, 126.1, 126.0, 125.3, 122.7, 121.4, 116.2, 112.4, 112.4, 67.6, 56.0, 25.2. HR-MS (ESI) *m/z*: calcd for C$_{21}$H$_{20}$N$_2$NaO$_4$ [M + Na]$^+$ 387.1315 found 387.1315.

N-hydroxy-3-(2-methoxy-5-(1-(2-methylquinolin-4-yl)vinyl)phenoxy)propanamide (II-19e). White solid, yield 33%. ^{1}H NMR (300 MHz, DMSO-d_6) δ 10.55 (s, 1H), 8.86 (s, 1H), 7.94 (d, J = 8.3 Hz, 1H), 7.64 (ddd, J = 8.3, 6.8, 1.4 Hz, 1H), 7.58 (d, J = 8.4 Hz, 1H), 7.41 – 7.33 (m, 1H), 7.31 (s, 1H), 7.11 (d, J = 2.2 Hz, 1H), 6.80 (d, J = 8.5 Hz, 1H), 6.48 (dd, J = 8.3, 2.0 Hz, 1H), 6.04 (s, 1H), 5.29 (s, 1H), 4.13 (t, J = 6.0 Hz, 2H), 3.69 (s, 3H), 2.68 (s, 3H), 2.41 (t, J = 5.9 Hz, 2H). ^{13}C NMR (100 MHz, DMSO-d_6) δ 166.9, 159.1, 149.6, 148.3, 148.3, 148.1, 145.5, 132.5, 129.7, 129.2, 126.1, 126.1, 125.3, 122.7, 120.4, 116.2, 112.2, 111.2, 65.0, 55.9, 33.0, 25.3. HR-MS (ESI) *m/z*: calcd for C$_{22}$H$_{23}$N$_2$O$_4$ [M + H]$^+$ 379.1652 found 379.1655.

N-hydroxy-4-(2-methoxy-5-(1-(2-methylquinolin-4-yl)vinyl)phenoxy)butanamide (II-19f). Yellow solid, yield 78%. ^{1}H NMR (300 MHz, DMSO-d_6) δ 10.44 (s, 1H), 8.73

(s, 1H), 7.93 (d, J = 8.4 Hz, 1H), 7.64 (ddd, J = 8.4, 6.8, 1.4 Hz, 1H), 7.57 (dd, J = 8.4, 1.3 Hz, 1H), 7.37 (ddd, J = 8.3, 6.8, 1.3 Hz, 1H), 7.31 (s, 1H), 7.12 (d, J = 2.1 Hz, 1H), 6.80 (d, J = 8.5 Hz, 1H), 6.44 (dd, J = 8.4, 2.1 Hz, 1H), 6.03 (s, 1H), 5.29 (s, 1H), 3.93 (t, J = 6.2 Hz, 2H), 3.70 (s, 3H), 2.68 (s, 3H), 2.11 (t, J = 7.4 Hz, 2H), 1.89 (p, J = 6.7 Hz, 2H). ^{13}C NMR (75 MHz, DMSO-d_6) δ 169.2, 159.1, 149.8, 148.5, 148.3, 148.0, 145.5, 132.4, 129.7, 129.1, 126.1, 126.1, 125.3, 122.7, 120.4, 116.1, 112.1, 111.2, 68.2, 55.9, 29.2, 25.3, 25.2. HR-MS (ESI) m/z: calcd for $C_{23}H_{24}N_2NaO_4$ [M + Na]$^+$ 415.1628 found 415.1635.

N-hydroxy-5-(2-methoxy-5-(1-(2-methylquinolin-4-yl)vinyl)phenoxy)pentanamide (II-19g). Yellow solid, yield 64%. ^{1}H NMR (300 MHz, DMSO-d_6) δ 10.55 (s, 1H), 8.79 (s, 1H), 7.97 (d, J = 8.3 Hz, 1H), 7.75 – 7.66 (m, 1H), 7.66 – 7.58 (m, 1H), 7.41 (ddd, J = 8.2, 6.8, 1.2 Hz, 1H), 7.34 (s, 1H), 7.14 (d, J = 2.1 Hz, 1H), 6.82 (d, J = 8.4 Hz, 1H), 6.48 (dd, J = 8.4, 2.0 Hz, 1H), 6.07 (s, 1H), 5.32 (s, 1H), 4.00 – 3.91 (m, 2H), 3.74 (s, 3H), 2.71 (s, 3H), 2.05 (t, J = 6.7 Hz, 2H), 2.01 (s, 2H), 1.19 (t, J = 7.1 Hz, 2H). ^{13}C NMR (75 MHz, DMSO-d_6) δ 169.4, 159.1, 149.7, 148.6, 148.4, 148.1, 145.6, 132.4, 129.7, 129.1, 126.1, 125.3, 122.7, 120.2, 112.1, 111.0, 68.3, 60.2, 56.0, 32.4, 25.3, 14.6. HR-MS (ESI) m/z: calcd for $C_{24}H_{26}N_2NaO_4$ [M + Na]$^+$ 429.1785 found 429.1785.

N-hydroxy-6-(2-methoxy-5-(1-(2-methylquinolin-4-yl)vinyl)phenoxy)hexanamide (II-19h). Yellow solid, yield 81%. ^{1}H NMR (400 MHz, DMSO-d_6) δ 10.38 (s, 1H), 8.71 (s, 1H), 7.93 (d, J = 8.4 Hz, 1H), 7.76 – 7.52 (m, 2H), 7.49 – 7.25 (m, 2H), 7.05 (s, 1H), 6.80 (dd, J = 8.4, 2.3 Hz, 1H), 6.48 (d, J = 8.4 Hz, 1H), 6.02 (s, 1H), 5.29 (s, 1H), 3.89 (t, J = 6.7 Hz, 2H), 3.70 (d, J = 2.4 Hz, 3H), 2.68 (s, 3H), 1.94 (s, 2H), 1.68 – 1.28 (m, 6H). ^{13}C NMR (100 MHz, DMSO-d_6) δ 169.5, 159.1, 149.7, 148.6, 148.4, 148.0, 145.6, 132.4, 129.7, 129.1, 126.1, 125.3, 122.7, 120.1, 116.0, 112.1, 111.1, 68.6, 55.9, 32.7, 28.9, 25.6, 25.4, 25.2. HR-MS (ESI) m/z: calcd for $C_{25}H_{28}N_2NaO_4$ [M + Na]$^+$ 443.1941 found 443.1949.

N-hydroxy-2-(2-methoxy-5-(1-(2-methylquinolin-4-yl)vinyl)phenoxy)propanamide (II-19i). Yellow solid, yield 44%. ^{1}H NMR (300 MHz, DMSO-d_6) δ 10.83 (s, 1H), 9.04 (s, 1H), 7.98 (d, J = 8.4 Hz, 1H), 7.69 (dd, J = 5.4, 3.8 Hz, 1H), 7.65 – 7.58 (m, 1H), 7.44 (s, 1H), 7.33 (s, 1H), 7.17 (d, J = 2.1 Hz, 1H), 6.87 (d, J = 8.5 Hz, 1H), 6.55 (dd,

$J = 8.4, 2.1$ Hz, 1H), 5.99 (s, 1H), 5.34 (s, 1H), 4.65 (q, $J = 6.5$ Hz, 1H), 3.76 (s, 3H), 2.72 (s, 3H), 1.42 (d, $J = 6.5$ Hz, 3H). ^{13}C NMR (75 MHz, DMSO-d_6) δ 168.1, 159.1, 150.3, 148.1, 147.0, 145.3, 132.3, 129.7, 129.2, 126.1, 126.0, 125.2, 122.7, 121.5, 116.2, 113.8, 112.5, 73.8, 56.0, 25.3, 19.2. HR-MS (ESI) m/z: calcd for $C_{22}H_{22}N_2NaO_4$ [M + Na]$^+$ 401.1472 found 401.1481.

N-hydroxy-2-(2-methoxy-5-(1-(2-methylquinolin-4-yl)vinyl)phenoxy)-2-methylpropanamide (II-19j). Yellow solid, yield 35%. ^{1}H NMR (300 MHz, DMSO-d_6) δ 10.89 (s, 1H), 9.08 (s, 1H), 7.93 (d, $J = 8.3$ Hz, 1H), 7.64 (ddd, $J = 8.4, 6.7, 1.5$ Hz, 1H), 7.56 (dd, $J = 8.4, 1.3$ Hz, 1H), 7.41 – 7.32 (m, 1H), 7.28 (s, 1H), 6.81 (d, $J = 8.4$ Hz, 1H), 6.68 (d, $J = 2.2$ Hz, 1H), 6.63 (dd, $J = 8.4, 2.2$ Hz, 1H), 5.88 (s, 1H), 5.23 (s, 1H), 3.71 (s, 3H), 3.16 (s, 6H), 2.66 (s, 3H). ^{13}C NMR (100 MHz, DMSO-d_6) δ 159.2, 148.6, 148.3, 147.9, 146.8, 145.6, 132.6, 129.7, 129.0, 126.1, 126.1, 125.3, 122.6, 118.0, 115.5, 113.8, 112.5, 55.9, 49.1, 25.2. HR-MS (ESI) m/z: calcd for $C_{23}H_{25}N_2O_4$ [M + H]$^+$ 393.1809 found 393.1809.

2-fluoro-N-hydroxy-2-(2-methoxy-5-(1-(2-methylquinolin-4-yl)vinyl)phenoxy)acetamide (II-19k). Yellow solid, yield 67%. ^{1}H NMR (300 MHz, DMSO-d_6) δ 10.79 (s, 1H), 9.01 (s, 1H), 7.94 (d, $J = 8.4$ Hz, 1H), 7.69 – 7.61 (m, 1H), 7.61 – 7.55 (m, 1H), 7.43 – 7.33 (m, 2H), 7.31 (s, 1H), 6.89 (d, $J = 8.6$ Hz, 1H), 6.65 (dd, $J = 8.4, 2.2$ Hz, 1H), 6.37 (s, 1H), 6.01 (s, 1H), 5.37 (s, 1H), 3.73 (s, 3H), 2.68 (s, 3H). ^{13}C NMR (100 MHz, DMSO-d_6) δ 159.1, 148.5, 148.3, 148.1, 146.8, 145.7, 132.7, 129.7, 129.1, 126.08 (d, $J = 2.5$ Hz), 125.3, 122.6, 118.0, 115.5, 113.9, 112.6, 56.0, 25.3. HR-MS (ESI) m/z: calcd for $C_{21}H_{20}FN_2O_4$ [M + H]$^+$ 383.1402 found 383.1407. The purity of compound **II-19k** was 98% (t_R = 5.409 min), which was estimated by HPLC (SHIMADZU Labsolutions, UV detection at λ = 254 nm) analysis on the Aglilent C18 column (4.6 × 150 mm, 5 μm) eluting at 1 mL/min of 75% methanol/25% water.

2,2-difluoro-N-hydroxy-2-(2-methoxy-5-(1-(2-methylquinolin-4-yl)vinyl)phenoxy)acetamide (II-19l). White solid, yield 30%. ^{1}H NMR (300 MHz, DMSO-d_6) δ 11.83 (s, 1H), 9.54 (s, 1H), 7.95 (d, $J = 8.4$ Hz, 1H), 7.66 (ddd, $J = 8.4, 6.7, 1.5$ Hz, 1H), 7.55 (d, $J = 8.2$ Hz, 1H), 7.40 (ddd, $J = 8.3, 6.7, 1.3$ Hz, 1H), 7.33 (s, 1H), 7.12 (d, $J = 10.6$ Hz, 3H), 6.03 (s, 1H), 5.37 (s, 1H), 3.78 (s, 3H), 2.68 (s, 3H). [13]C

NMR (150 MHz, DMSO-d_6) δ 159.2, 156.2 (d, J = 35.3 Hz), 152.3, 148.1, 147.6, 144.4, 137.8, 132.3, 129.8, 129.2, 126.3, 126.2, 125.8, 125.0, 122.7, 121.7, 117.2, 115.5, 113.9, 56.5, 25.3. HR-MS (ESI) m/z: calcd for $C_{21}H_{19}F_2N_2O_4$ [M + H]$^+$ 401.1307 found 401.1313.

N-hydroxy-2-(3-(1-(2-methylquinolin-4-yl)vinyl)phenoxy)acetamide **(II-19m)**. Yellow solid, yield 77%. ^{1}H NMR (300 MHz, DMSO-d_6) δ 10.81 (s, 1H), 8.96 (s, 1H), 7.95 (d, J = 8.4 Hz, 1H), 7.66 (t, J = 7.8 Hz, 1H), 7.57 (d, J = 8.3 Hz, 1H), 7.39 (t, J = 7.8 Hz, 1H), 7.32 (s, 1H), 7.22 (t, J = 7.9 Hz, 1H), 7.03 – 6.84 (m, 2H), 6.79 (d, J = 7.8 Hz, 1H), 6.11 (s, 1H), 5.43 (s, 1H), 4.44 (s, 2H), 2.69 (s, 3H). ^{13}C NMR (100 MHz, DMSO-d_6) δ 164.6, 159.2, 158.4, 148.1, 147.8, 145.6, 141.2, 130.2, 129.8, 129.2, 126.2, 125.9, 125.1, 122.8, 119.9, 118.4, 114.3, 113.5, 66.3, 25.3. HR-MS (ESI) m/z: calcd for $C_{20}H_{19}N_2O_3$ [M + H]$^+$ 335.1390 found 335.1390.

N-hydroxy-2-(3-(1-(2-methylquinolin-4-yl)vinyl)phenoxy)propanamide **(II-19n)**. Yellow solid, yield 67%. ^{1}H NMR (300 MHz, DMSO-d_6) δ 10.94 (s, 1H), 8.68 (s, 1H), 7.95 (dd, J = 8.5, 1.2 Hz, 1H), 7.73 – 7.60 (m, 1H), 7.61 – 7.53 (m, 1H), 7.41 (d, J = 1.3 Hz, 1H), 7.31 (s, 1H), 7.19 (t, J = 7.9 Hz, 1H), 6.95 – 6.82 (m, 2H), 6.82 – 6.73 (m, 1H), 6.15 – 6.05 (m, 1H), 5.42 (s, 1H), 4.70 (d, J = 6.6 Hz, 1H), 2.68 (s, 3H), 1.36 (d, J = 6.5 Hz, 3H). ^{13}C NMR (100 MHz, DMSO-d_6) δ 167.9, 159.2, 157.8, 148.1, 147.9, 145.5, 141.1, 130.2, 129.8, 129.2, 126.2, 125.9, 125.1, 122.8, 119.7, 118.3, 114.7, 114.1, 72.3, 25.3, 19.2. HR-MS (ESI) m/z: calcd for $C_{21}H_{21}N_2O_3$ [M + H]$^+$ 349.1547 found 349.1551.

N-hydroxy-2-methyl-2-(3-(1-(2-methylquinolin-4-yl)vinyl)phenoxy)propanamide **(II-19o)**. White solid, yield 17%. ^{1}H NMR (300 MHz, DMSO-d_6) δ 10.87 (s, 1H), 8.87 (s, 1H), 7.99 (d, J = 8.3 Hz, 1H), 7.70 (ddd, J = 8.4, 6.7, 1.5 Hz, 1H), 7.58 (td, J = 8.3, 1.4 Hz, 1H), 7.42 (tdd, J = 7.2, 4.0, 2.1 Hz, 1H), 7.36 (s, 1H), 7.31 – 7.19 (m, 1H), 7.10 – 6.91 (m, 1H), 6.87 – 6.76 (m, 2H), 6.10 (s, 1H), 5.47 (s, 1H), 2.73 (s, 3H), 1.41 (s, 3H), 1.39 (s, 3H). ^{13}C NMR (125 MHz, DMSO-d_6) δ 170.3, 159.2, 155.5, 148.1, 147.8, 145.5, 141.0, 129.8, 129.2, 126.2, 125.9, 125.1, 122.8, 120.9, 120.6, 119.5, 118.6, 118.2, 80.1, 25.5, 25.3, 24.2. HR-MS (ESI) m/z: calcd for $C_{22}H_{23}N_2O_3$ [M + H]$^+$ 363.1703 found 363.1703.

N-hydroxy-4-(3-(1-(2-methylquinolin-4-yl)vinyl)phenoxy)butanamide **(II-19p)**. White solid, yield 60%. ^{1}H NMR (300 MHz, DMSO-d_6) δ 10.39 (s, 1H), 8.71 (s, 1H), 7.94 (d, J = 8.4 Hz, 1H), 7.65 (ddd, J = 8.4, 6.7, 1.5 Hz, 1H), 7.57 (dd, J = 8.4, 1.4 Hz, 1H), 7.38 (ddd, J = 8.2, 6.7, 1.2 Hz, 1H), 7.32 (s, 1H), 7.20 (t, J = 7.9 Hz, 1H), 6.91 – 6.81 (m, 2H), 6.74 (d, J = 7.8 Hz, 1H), 6.11 (s, 1H), 5.42 (s, 1H), 3.91 (t, J = 6.3 Hz, 2H), 2.68 (s, 3H), 2.08 (t, J = 7.4 Hz, 2H), 1.88 (q, J = 6.9 Hz, 2H). ^{13}C NMR (100 MHz, DMSO-d_6) δ 169.0, 159.2, 159.2, 148.1, 147.9, 145.7, 141.2, 130.3, 129.7, 129.2, 126.2, 125.9, 125.1, 122.8, 119.3, 118.2, 114.2, 113.0, 67.3, 29.2, 25.3, 25.2. HR-MS (ESI) *m/z*: calcd for $C_{22}H_{23}N_2O_3$ [M + H]$^+$ 363.1703 found 363.1703.

(E)-N-hydroxy-4-(3-(1-(2-methylquinolin-4-yl)vinyl)phenoxy)but-2-enamide **(II-19q)**. White solid, yield 15%. ^{1}H NMR (300 MHz, DMSO-d_6) δ 10.68 (s, 1H), 9.00 (s, 1H), 7.95 (d, J = 8.3 Hz, 1H), 7.66 (ddd, J = 8.4, 6.7, 1.5 Hz, 1H), 7.56 (dd, J = 8.3, 1.4 Hz, 1H), 7.41 (d, J = 1.3 Hz, 1H), 7.33 (s, 1H), 7.23 (t, J = 7.8 Hz, 1H), 6.90 (d, J = 7.9 Hz, 2H), 6.77 (d, J = 8.0 Hz, 2H), 6.12 (s, 1H), 6.01 (d, J = 15.6 Hz, 1H), 5.43 (s, 1H), 4.71 (dd, J = 4.3, 1.9 Hz, 2H), 2.68 (s, 3H). ^{13}C NMR (125 MHz, DMSO-d_6) δ 162.3, 159.2, 158.6, 148.1, 147.9, 145.6, 141.3, 137.0, 130.4, 129.8, 129.2, 126.2, 125.9, 125.1, 122.8, 122.0, 119.7, 118.4, 114.5, 113.3, 66.9, 25.3. HR-MS (ESI) *m/z*: calcd for $C_{22}H_{21}N_2O_3$ [M + H]$^+$ 361.1547 found 361.1547.

N-hydroxy-6-(3-(1-(2-methylquinolin-4-yl)vinyl)phenoxy)hexanamide **(II-19r)**. Yellow solid, yield 61%. ^{1}H NMR (300 MHz, DMSO-d_6) δ 10.33 (s, 1H), 8.68 (s, 1H), 7.94 (d, J = 8.3 Hz, 1H), 7.65 (ddd, J = 8.3, 6.8, 1.4 Hz, 1H), 7.56 (d, J = 8.3 Hz, 1H), 7.38 (t, J = 7.6 Hz, 1H), 7.32 (s, 1H), 7.19 (t, J = 7.9 Hz, 1H), 6.91 – 6.80 (m, 2H), 6.74 (d, J = 7.7 Hz, 1H), 6.11 (s, 1H), 5.41 (s, 1H), 3.88 (t, J = 6.3 Hz, 2H), 2.68 (s, 3H), 1.93 (t, J = 7.2 Hz, 2H), 1.62 (t, J = 7.3 Hz, 2H), 1.50 (p, J = 7.3 Hz, 2H), 1.44 – 1.25 (m, 2H). ^{13}C NMR (100 MHz, DMSO-d_6) δ 169.5, 159.3, 159.2, 148.1, 148.0, 145.8, 141.2, 130.2, 129.7, 129.2, 126.2, 125.9, 125.1, 122.8, 119.2, 118.2, 114.2, 113.0, 67.8, 32.7, 28.8, 25.6, 25.4, 25.3. HR-MS (ESI) *m/z*: calcd for $C_{24}H_{27}N_2O_3$ [M + H]$^+$ 391.2016 found 391.2016.

N-hydroxy-2-(2-methoxy-5-(1-(quinolin-4-yl)vinyl)phenoxy)acetamide **(II-19s)**. Yellow solid, yield 58%. ^{1}H NMR (300 MHz, DMSO-d_6) δ 10.78 (s, 1H), 9.07 – 8.99

(m, 1H), 8.93 (d, J = 4.3 Hz, 1H), 8.06 (d, J = 8.4 Hz, 1H), 7.75 – 7.70 (m, 1H), 7.65 (d, J = 1.7 Hz, 1H), 7.49 (dd, J = 6.6, 1.8 Hz, 1H), 7.40 (d, J = 4.3 Hz, 1H), 7.21 (d, J = 2.2 Hz, 1H), 6.83 (d, J = 8.4 Hz, 1H), 6.48 (dd, J = 8.4, 2.1 Hz, 1H), 6.03 (s, 1H), 5.31 (s, 1H), 4.45 (s, 2H), 3.73 (s, 3H). ^{13}C NMR (75 MHz, DMSO-d_6) δ 167.5, 164.8, 150.9, 150.0, 148.4, 148.1, 148.0, 145.2, 132.2, 132.0, 129.9, 129.1, 127.1, 126.9, 126.3, 122.1, 121.4, 112.4, 67.9, 56.0. HR-MS (ESI) m/z: calcd for $C_{20}H_{19}N_2O_4$ [M + H]$^+$ 351.1339 found 351.1339.

N-hydroxy-2-(2-methoxy-5-(1-(quinolin-4-yl)vinyl)phenoxy)propanamide (II-19t). White solid, yield 74%. ^{1}H NMR (300 MHz, DMSO-d_6) δ 10.78 (s, 1H), 8.97 (s, 1H), 8.93 (d, J = 4.3 Hz, 1H), 8.05 (d, J = 8.4 Hz, 1H), 7.77 – 7.60 (m, 2H), 7.47 (t, J = 7.7 Hz, 1H), 7.39 (d, J = 4.3 Hz, 1H), 7.13 (d, J = 2.2 Hz, 1H), 6.83 (d, J = 8.4 Hz, 1H), 6.49 (dd, J = 8.4, 2.1 Hz, 1H), 5.99 (s, 1H), 5.31 (s, 1H), 4.62 (d, J = 6.6 Hz, 1H), 3.72 (s, 3H), 1.16 (t, J = 7.1 Hz, 3H). ^{13}C NMR (100 MHz, DMSO-d_6) δ 168.0, 150.9, 150.4, 148.4, 147.0, 145.2, 132.3, 132.1, 129.9, 129.8, 129.1, 127.1, 126.3, 122.1, 121.5, 116.4, 113.8, 112.6, 73.8, 56.0, 19.2. HR-MS (ESI) m/z: calcd for $C_{21}H_{20}N_2NaO_4$ [M + Na]$^+$ 387.1315 found 387.1315.

N-hydroxy-4-(2-methoxy-5-(1-(quinolin-4-yl)vinyl)phenoxy)butanamide (II-19u). White solid, yield 55%. ^{1}H NMR (300 MHz, DMSO-d_6) δ 10.52 (s, 1H), 8.97 (d, J = 4.3 Hz, 1H), 8.78 (s, 1H), 8.09 (dd, J = 8.5, 1.1 Hz, 1H), 7.89 – 7.61 (m, 2H), 7.50 (ddd, J = 8.3, 6.8, 1.3 Hz, 1H), 7.44 (d, J = 4.3 Hz, 1H), 7.16 (d, J = 2.2 Hz, 1H), 6.83 (d, J = 8.5 Hz, 1H), 6.48 (dd, J = 8.3, 2.1 Hz, 1H), 6.10 (s, 1H), 5.34 (s, 1H), 3.97 (t, J = 6.3 Hz, 2H), 3.74 (s, 3H), 2.16 (t, J = 7.3 Hz, 2H), 1.95 (q, J = 6.8 Hz, 2H). ^{13}C NMR (75 MHz, DMSO-d_6) δ 169.2, 150.9, 149.8, 148.5, 148.4, 148.3, 145.4, 132.4, 129.9, 129.8, 127.1, 126.9, 126.3, 122.1, 120.4, 116.3, 112.1, 111.1, 68.2, 56.0, 29.2, 25.3. HR-MS (ESI) m/z: calcd for $C_{22}H_{22}N_2NaO_4$ [M + Na]$^+$ 401.1472 found 401.1475.

N-hydroxy-6-(2-methoxy-5-(1-(quinolin-4-yl)vinyl)phenoxy)hexanamide (II-19v). Gray solid, yield 67%. ^{1}H NMR (400 MHz, DMSO-d_6) δ 10.39 (s, 1H), 9.16 – 8.82 (m, 1H), 8.73 (s, 1H), 8.07 (d, J = 8.4 Hz, 1H), 7.87 – 7.54 (m, 2H), 7.58 – 7.29 (m, 2H), 7.07 (s, 1H), 6.81 (s, 1H), 6.50 (d, J = 8.6 Hz, 1H), 6.07 (s, 1H), 5.30 (d, J = 14.0 Hz, 1H), 3.95 – 3.81 (m, 2H), 3.72 (s, 3H), 2.05 – 1.68 (m, 2H), 1.68 – 1.43 (m, 4H), 1.46

– 1.06 (m, 2H). ^{13}C NMR (100 MHz, DMSO-d_6) δ 169.5, 150.9, 149.7, 148.6, 148.4, 148.3, 145.4, 132.4, 129.9, 129.8, 127.1, 126.9, 126.3, 122.1, 120.1, 116.3, 112.1, 111.0, 68.6, 55.9, 32.7, 28.9, 25.6, 25.4. HR-MS (ESI) m/z: calcd for $C_{24}H_{26}N_2NaO_4$ [M + Na]$^+$ 429.1785 found 429.1785.

*N-hydroxy-2-(2-methoxy-5-(1-(2-methylpyridin-4-yl)vinyl)phenoxy)acetamide (**II-25a**)*. Yellow solid, yield 48%. ^{1}H NMR (300 MHz, DMSO-d_6) δ 10.80 (s, 1H), 9.08 (s, 1H), 8.45 (d, J = 5.2 Hz, 1H), 7.19 (d, J = 1.6 Hz, 1H), 7.10 (dd, J = 5.1, 1.7 Hz, 1H), 7.06 – 6.94 (m, 2H), 6.82 (dd, J = 8.4, 2.1 Hz, 1H), 5.59 (d, J = 6.5 Hz, 2H), 4.46 (s, 2H), 3.82 (s, 3H), 2.49 (s, 3H). ^{13}C NMR (75 MHz, DMSO-d_6) δ 164.8, 158.6, 149.9, 149.5, 148.8, 147.6, 147.2, 132.2, 122.3, 122.2, 120.3, 116.6, 114.3, 112.5, 67.3, 56.1, 24.5. HR-MS (ESI) m/z: calcd for $C_{17}H_{19}N_2O_4$ [M + H]$^+$ 315.1339 found 315.1339.

N-hydroxy-2-(2-methoxy-5-(1-(2-methylpyridin-4-yl)vinyl)phenoxy)propanamide (**II-25b**). Yellow solid, yield 59%. ^{1}H NMR (300 MHz, DMSO-d_6) δ 11.30 (s, 1H), 9.52 (s, 1H), 8.98 (d, J = 5.2 Hz, 1H), 7.71 (d, J = 1.6 Hz, 1H), 7.62 (dd, J = 5.1, 1.7 Hz, 1H), 7.54 (d, J = 8.4 Hz, 1H), 7.47 (d, J = 2.1 Hz, 1H), 7.37 (dd, J = 8.4, 2.1 Hz, 1H), 6.11 (s, 2H), 5.14 (q, J = 6.5 Hz, 1H), 4.36 (s, 3H), 3.02 (s, 3H), 1.97 (d, J = 6.6 Hz, 3H). ^{13}C NMR (100 MHz, DMSO-d_6) δ 168.0, 158.6, 150.3, 149.5, 148.8, 147.1, 146.8, 132.1, 122.4, 122.3, 120.3, 116.5, 115.8, 112.6, 73.8, 56.1, 24.5, 19.3. HR-MS (ESI) m/z: calcd for $C_{18}H_{21}N_2O_4$ [M + H]$^+$ 329.1496 found 329.1501.

N-hydroxy-4-(2-methoxy-5-(1-(2-methylpyridin-4-yl)vinyl)phenoxy)butanamide (**II-25c**). Yellow solid, yield 66%. ^{1}H NMR (300 MHz, DMSO-d_6) δ 10.48 (s, 1H), 8.77 (s, 1H), 8.45 (d, J = 5.2 Hz, 1H), 7.19 (s, 1H), 7.10 (d, J = 5.2 Hz, 1H), 7.02 – 6.89 (m, 2H), 6.86 – 6.63 (m, 1H), 5.59 (d, J = 16.4 Hz, 2H), 3.95 (t, J = 6.3 Hz, 2H), 3.81 (s, 3H), 2.49 (s, 3H), 2.16 (t, J = 7.3 Hz, 2H), 1.94 – 1.83 (m, 2H). ^{13}C NMR (75 MHz, DMSO-d_6) δ 169.1, 158.6, 149.7, 149.5, 149.0, 148.2, 147.4, 132.4, 122.3, 121.2, 120.3, 116.4, 113.2, 112.3, 68.2, 56.0, 29.2, 25.4, 24.5. HR-MS (ESI) m/z: calcd for $C_{19}H_{23}N_2O_4$ [M + H]$^+$ 343.1652 found 343.1652.

N-hydroxy-6-(2-methoxy-5-(1-(2-methylpyridin-4-yl)vinyl)phenoxy)hexanamide (**II-25d**). Yellow solid, yield 70%. ^{1}H NMR (400 MHz, DMSO-d_6) δ 10.38 (s, 1H), 8.72 (s, 1H), 8.45 (d, J = 5.1 Hz, 1H), 7.24 – 7.15 (m, 1H), 7.10 (dd, J = 5.1, 1.6 Hz, 1H),

6.98 (d, $J = 8.4$ Hz, 1H), 6.90 (d, $J = 2.1$ Hz, 1H), 6.76 (dd, $J = 8.3, 2.1$ Hz, 1H), 5.62 (s, 1H), 5.56 (s, 1H), 3.93 (t, $J = 6.4$ Hz, 2H), 3.80 (s, 3H), 2.55 – 2.51 (m, 3H), 1.98 (t, $J = 7.3$ Hz, 2H), 1.70 (q, $J = 7.0$ Hz, 2H), 1.55 (q, $J = 7.5$ Hz, 2H), 1.39 (qd, $J = 7.8, 7.3, 4.2$ Hz, 2H). ^{13}C NMR (75 MHz, DMSO-d_6) δ 169.5, 158.6, 149.6, 149.5, 149.1, 148.4, 147.4, 132.4, 122.3, 121.0, 120.3, 116.4, 112.9, 112.2, 68.5, 56.0, 32.7, 29.0, 25.6, 25.4, 24.5. HR-MS (ESI) *m/z*: calcd for $C_{21}H_{25}N_2NaO_4$ [M + Na]$^+$ 393.1785 found 393.1785.

N-hydroxy-2-(2-methoxy-5-(1-(2-methoxypyridin-4-yl)vinyl)phenoxy)acetamide (***II-25e***). White solid, yield 45%. ^{1}H NMR (300 MHz, DMSO-d_6) δ 8.17 (d, $J = 5.3$ Hz, 1H), 7.05 – 6.95 (m, 2H), 6.90 (dd, $J = 5.3, 1.5$ Hz, 1H), 6.82 (dd, $J = 8.3, 2.0$ Hz, 1H), 6.70 (d, $J = 1.3$ Hz, 1H), 5.60 (d, $J = 6.8$ Hz, 2H), 4.47 (s, 2H), 3.88 (s, 3H), 3.82 (s, 3H). ^{13}C NMR (75 MHz, DMSO-d_6) δ 164.8, 164.5, 151.8, 149.9, 147.7, 147.4, 146.8, 132.1, 122.1, 116.9, 116.7, 114.3, 112.4, 109.5, 67.3, 56.1, 53.7. HR-MS (ESI) *m/z*: calcd for $C_{17}H_{18}N_2NaO_5$ [M + Na]$^+$ 353.1108 found 353.1108.

*N-hydroxy-2-(2-methoxy-5-(1-(2-methoxypyridin-4-yl)vinyl)phenoxy)propanamide (**II-25f**)*. White solid, yield 39%. ^{1}H NMR (300 MHz, DMSO-d_6) δ 10.75 (s, 1H), 8.95 (s, 1H), 8.13 (d, $J = 5.3$ Hz, 1H), 7.01 – 6.88 (m, 2H), 6.88 – 6.75 (m, 2H), 6.67 (d, $J = 1.5$ Hz, 1H), 5.55 (d, $J = 2.5$ Hz, 2H), 4.58 (q, $J = 6.5$ Hz, 1H), 3.85 (s, 3H), 3.79 (s, 3H), 1.40 (d, $J = 6.5$ Hz, 3H). ^{13}C NMR (75 MHz, DMSO-d_6) δ 168.1, 164.5, 151.7, 150.3, 147.4, 146.8, 146.8, 132.0, 122.4, 116.9, 116.7, 115.8, 112.6, 109.5, 73.9, 56.1, 53.7, 19.3. HR-MS (ESI) *m/z*: calcd for $C_{18}H_{20}N_2NaO_5$ [M + Na]$^+$ 367.1264 found 367.1264.

*N-hydroxy-4-(2-methoxy-5-(1-(2-methoxypyridin-4-yl)vinyl)phenoxy)butanamide (**II-25g**)*. White solid, yield 80%. ^{1}H NMR (300 MHz, DMSO-d_6) δ 10.43 (s, 1H), 8.72 (s, 1H), 8.12 (d, $J = 5.3$ Hz, 1H), 6.98 – 6.83 (m, 3H), 6.73 (dd, $J = 8.2, 2.0$ Hz, 1H), 6.66 (d, $J = 1.4$ Hz, 1H), 5.56 (d, $J = 12.8$ Hz, 2H), 4.04 – 3.89 (m, 2H), 3.84 (s, 3H), 3.77 (s, 3H), 2.12 (t, $J = 7.4$ Hz, 2H), 1.92 (td, $J = 13.8, 13.1, 6.3$ Hz, 2H). ^{13}C NMR (75 MHz, DMSO-d_6) δ 169.1, 164.5, 152.0, 149.7, 148.3, 147.3, 147.0, 132.2, 121.2, 116.9, 116.6, 113.1, 112.2, 109.6, 68.2, 56.0, 53.7, 29.2, 25.4. HR-MS (ESI) *m/z*: calcd for $C_{19}H_{22}N_2NaO_5$ [M + Na]$^+$ 381.1421 found 381.1421.

N-hydroxy-6-(2-methoxy-5-(1-(2-methoxypyridin-4-yl)vinyl)phenoxy)hexanamide (II-25h). Brown oil, yield 45%. ^{1}H NMR (300 MHz, DMSO-d_6) δ 10.36 (s, 1H), 8.69 (s, 1H), 8.12 (d, $J = 5.3$ Hz, 1H), 7.00 – 6.79 (m, 3H), 6.74 (d, $J = 2.0$ Hz, 1H), 6.66 (d, $J = 1.3$ Hz, 1H), 5.55 (d, $J = 13.1$ Hz, 2H), 3.89 (t, $J = 6.4$ Hz, 2H), 3.84 (s, 3H), 3.76 (s, 3H), 1.95 (t, $J = 7.3$ Hz, 2H), 1.67 (p, $J = 6.8$ Hz, 2H), 1.51 (q, $J = 7.4$ Hz, 2H), 1.41 – 1.27 (m, 2H). ^{13}C NMR (100 MHz, DMSO-d_6) δ 169.5, 164.5, 152.0, 149.6, 148.4, 147.3, 147.1, 132.2, 121.0, 116.9, 116.5, 112.9, 112.1, 109.5, 68.5, 56.0, 53.6, 32.7, 29.0, 25.7, 25.4. HR-MS (ESI) *m/z*: calcd for $C_{21}H_{26}N_2NaO_5$ [M + Na]$^+$ 409.1734 found 409.1734.

2-(5-(1-(2,6-dimethylpyridin-4-yl)vinyl)-2-methoxyphenoxy)-N-hydroxyacetamide (II-25i). White solid, yield 67%. ^{1}H NMR (300 MHz, DMSO-d_6) δ 10.83 (s, 1H), 8.98 (s, 1H), 7.08 – 6.91 (m, 4H), 6.81 (dd, $J = 8.3, 2.1$ Hz, 1H), 5.56 (d, $J = 11.0$ Hz, 2H), 4.47 (s, 2H), 3.83 (s, 3H), 2.44 (s, 6H). ^{13}C NMR (75 MHz, DMSO-d_6) δ 164.8, 157.8, 149.8, 149.3, 147.6, 147.4, 132.4, 122.1, 119.5, 116.2, 114.3, 112.5, 67.3, 56.1, 24.4. HR-MS (ESI) *m/z*: calcd for $C_{18}H_{21}N_2O_4$ [M + H]$^+$ 329.1496 found 329.1496.

2-(5-(1-(2,6-dimethylpyridin-4-yl)vinyl)-2-methoxyphenoxy)-N-hydroxypropanamide (II-25j). Yellow oil, yield 33%. ^{1}H NMR (300 MHz, DMSO-d_6) δ 10.78 (s, 1H), 9.04 (d, $J = 36.6$ Hz, 1H), 7.75 – 7.70 (m, 1H), 6.96 (d, $J = 2.8$ Hz, 4H), 6.77 – 6.63 (m, 2H), 5.55 (d, $J = 5.0$ Hz, 1H), 3.81 (s, 3H), 2.44 (s, 6H), 1.44 (d, $J = 6.6$ Hz, 3H). ^{13}C NMR (100 MHz, DMSO-d_6) δ 167.4, 157.8, 157.7, 149.7, 148.2, 147.8, 146.7, 129.1, 122.4, 119.5, 119.4, 119.3, 115.4, 112.4, 67.8, 56.0, 24.4, 23.7. HR-MS (ESI) *m/z*: calcd for $C_{19}H_{23}N_2O_4$ [M + H]$^+$ 343.1652 found 343.1652.

4-(5-(1-(2,6-dimethylpyridin-4-yl)vinyl)-2-methoxyphenoxy)-N-hydroxybutanamide (II-25k). Brown oil, yield 42%. ^{1}H NMR (300 MHz, DMSO-d_6) δ 10.42 (s, 1H), 8.72 (s, 1H), 6.94 (d, $J = 7.8$ Hz, 3H), 6.88 (d, $J = 2.0$ Hz, 1H), 6.73 (dd, $J = 8.3, 2.0$ Hz, 1H), 5.52 (d, $J = 18.7$ Hz, 2H), 3.92 (t, $J = 6.3$ Hz, 2H), 3.77 (s, 3H), 2.40 (s, 6H), 2.12 (t, $J = 7.4$ Hz, 2H), 1.97 – 1.83 (m, 2H). ^{13}C NMR (100 MHz, DMSO-d_6) δ 167.4, 157.8, 157.7, 149.7, 148.2, 147.8, 146.7, 129.1, 119.5, 119.4, 119.3, 115.4, 112.4, 67.8, 56.0, 30.3, 28.8, 24.4. HR-MS (ESI) *m/z*: calcd for $C_{20}H_{25}N_2O_4$ [M + H]$^+$ 357.1809 found 357.1809.

6-(5-(1-(2,6-dimethylpyridin-4-yl)vinyl)-2-methoxyphenoxy)-N-

*hydroxyhexanamide (**II-25l**).* Yellow solid, yield 66%. ^{1}H NMR (400 MHz, DMSO-d_6)

δ 10.38 (s, 1H), 8.73 (s, 1H), 6.97 – 6.91 (m, 3H), 6.87 (d, J = 2.1 Hz, 1H), 6.73 (dd, J

= 8.3, 2.1 Hz, 1H), 5.61 – 5.44 (m, 2H), 3.90 (t, J = 6.4 Hz, 2H), 3.78 (s, 3H), 2.41 (s,

6H), 1.99 – 1.95 (m, 2H), 1.68 (q, J = 5.7, 4.1 Hz, 2H), 1.57 – 1.51 (m, 2H), 1.39 – 1.34

(m, 2H). ^{13}C NMR (100 MHz, DMSO-d_6) δ 169.5, 157.7, 149.6, 149.5, 148.3, 147.6,

132.5, 120.9, 119.5, 116.0, 112.9, 112.1, 68.5, 56.0, 32.7, 29.0, 25.7, 25.4, 24.4. HR-

MS (ESI) m/z: calcd for $C_{22}H_{28}N_2NaO_4$ [M + Na]$^+$ 407.1941 found 407.1941.

4.2 Biology

4.2.1 In Vitro Anti-proliferative Assay

The growth of tumor cells was determined using the MTT assay. In brief, the cells

(K562, MCF-7, MDA-MB-231, A549, B16F10, A2780 and HFL-1 cells) were cultured

in a 5% CO_2 humidified incubator at 37 °C for 24 h in 96-well plates before the

experiments. After removal of medium, 100 μL of medium containing the test

compounds at different concentrations was added to each well and incubated at 37 °C

for 72 h. MTT (5 mg/mL PBS) was added and incubated for 4 hours. Then the

supernatant was discarded, and 150 μL of DMSO was added (for K562 cells:

centrifugation at 1000 rpm for 10 min in advance). After shaken for 30 min in incubator

shaker, the number of living cells after culture in the presence (or absence, as in the

case of the control) of the various compounds was directly proportional to the intensity

of the blue color of media, which was quantitatively measured by spectrophotometry

(Biorad, Nazareth, Belgium) at a 490 nm wavelength. The experiment was repeated at

least three times independently.

4.2.2 HDAC Enzymes Inhibition Assay

The human tumor cell line Hela was obtained from the cell bank of Shanghai

Institute of Biological Sciences, Chinese Academy of Sciences. Hela cells were

cultured in MEM medium containing 10% fetal bovine serum, and the cells were

incubated in a 5% CO_2 environment at 37 °C. Cells were lysed with the buffer (150

mM NaCl, 50 mM Tris-HCl pH 7.4, 1% Triton x-100). The enzymatic reaction of Hela

cell extract was carried out at 37 °C for 0.5 h. The 50 μL reaction mixture contains 1

mM MgCl$_2$, 25 mM Tris pH 8.0, 0.1 mg/ml BSA, 2.7 mM KCl, 137 mM NaCl, the enzyme substrate (20 µM Ac-Leu-Gly-Lys(Ac)-AMC) and Hela extract. The test compound was diluted in 10% DMSO, and add 5 µL of the dilution to a 50 µL reaction to make a final concentration of 1% DMSO in all reactions. The amount of fluorescent product in solution was quantitatively analyzed after enzymatic reaction. At the end of the enzymatic reaction, 50 µL of 0.4 mg/mL trypsin was added to each well and incubated for another 15 min at room temperature. Fluorescence was analyzed on a SpectraMax M5 microplate reader using excitation at 350-360 nm and emission at 450-460 nm. The IC$_{50}$ values were calculated by nonlinear regression of the normalized dose-effect fit using Prism GraphPad software.

All the enzymatic reactions were conducted for 0.5 h at 37 °C. The 50 µL reaction mixture contains 1 mM MgCl$_2$, 25 mM Tris, 0.1 mg/mL BSA, 2.7 mM KCl, 137 mM NaCl, the enzyme substrate and HDAC. The test compound was diluted in 10% DMSO, and add 5 µL of the dilution to a 50 µL reaction to make a final concentration of 1% DMSO in all reactions. The amount of fluorescent product in solution was quantitatively analyzed after enzymatic reaction. Fluorescence was analyzed on a SpectraMax M5 microplate reader using excitation at 350-360 nm and emission at 450-460 nm. The IC$_{50}$ values were calculated by nonlinear regression of the normalized dose-effect fit using Prism GraphPad software.

4.2.3 Western Blot Analysis

Cells were incubated with various concentrations of indicated compounds for 24 h, then lysed with ice lysis buffer for 0.5 h, followed by centrifugation at 14,000 rpm for 0.5 h. Protein concentrations were determined, and equal amounts of proteins were separated by 8-15% SDS-PAGE and transferred to PVDF membranes. Membranes were immunoblotted using specific antibodies overnight at 4 °C, and applied with horseradish peroxidase-conjugated secondary antibodies for 2 h at room temperature. Signal was detected with enhanced chemiluminescence and visualized by an imager. Gel-Pro32 software was used for data analysis.

4.2.4 Immunofluorescent Staining Assay

K562 cells were seeded into 6-well plates, and treated with vehicle control 0.1%

DMSO, and **II-19k** with different concentrations. Cells were fixed with 4% paraformaldehyde and washed three times with PBS. After blocking with 50–100 µL of goat serum albumin for 20 min at room temperature, the cells were incubated with anti-α-tubulin monoclonal antibody for 2 h at 37 °C. After staining with fluorescent secondary antibody and 4,6-diamidino-2-phenylindole (DAPI)-labeled nuclei, the cells were washed three times with PBS. Cells were observed under a Carl Zeiss LSM 570 laser scanning confocal microscope.

4.2.5 Cell Cycle Analysis

K562 cells were seeded into 6-well plates and cultured in a 5% CO_2 humidified incubator at 37 °C for 24 h, and treated with or without **II-19k** at indicated concentrations for another 48 h. The collected cells were fixed with 70% ethanol at 4 °C for 12 h. Subsequently, cells were resuspended in PBS containing 100 mL RNase A and 400 mL propidium iodide for 0.5 h. Cellular DNA content was detected using a FACS Calibur flow cytometer (Bectone Dickinson, San Jose, CA, USA).

4.2.6 Hoechst 33342 Staining

About 5×10^4 cells per well were seeded in 6-well culture plates, and then incubated with **II-19k** at indicated concentrations for 48 h. After incubation, cells were washed with PBS, fixed with 4% paraformaldehyde for 0.5 h, and then stained with 20 µg/mL Hoechst 33342 for 15 min at room temperature in the dark. The morphological changes of cells after **II-19k** treatment were observed by fluorescence microscope.

4.2.7 Cell Apoptosis Analysis

K562 cells were treated with or without **II-19k** at the indicated concentrations for 48 h, washed twice in PBS, centrifuged, and resuspended in 500 µL AnnexinV binding buffer. Cells were collected, washed, and stained with 5 mL Annexin V-APC and 5 mL 7-AAD for 15 min in the dark. Apoptosis was analyzed with a FACS Calibur flow cytometer (Bectone Dickinson, San Jose, CA, USA).

4.2.8 Mitochondrial Membrane Potential Analysis

After treatment of cells with vehicle control 0.1% DMSO and **II-19k** at indicated concentrations for 48 h, cells were washed in PBS and resuspended in 500 µL of JC-1 incubation buffer for 15 min at 37 °C. The percentage of cells with normal or collapsed

mitochondrial membrane potential was measured by flow cytometry (Bectone-Dickinson, San Jose, CA, USA).

4.2.9 Measurement of Intracellular ROS Generation

The production of intracellular reactive oxygen species (ROS) was detected by the peroxide-sensitive fluorescent probe DCF-DA. Briefly, K562 cells were treated with **II-19k** at indicated concentrations for 48 h and then incubated with 10 mM DCF-DA at 37 °C for 15 min. The intracellular ROS mediated oxidation of DCF-DA to the fluorescent compound 2′,7′-dichlorofluorescein (DCF). Cells were then collected and the cell pellet was suspended in 1 mL of PBS. Samples were analyzed by flow cytometry on an FC500 cytometer (Beckman Coulter) at an excitation wavelength of 480 nm and an emission wavelength of 525 nm.

4.2.10 Transwell Migration and Invasion Assay

In invasion experiments, diluted Matrigel was added to the upper chamber, while in migration experiments, the upper chamber was not coated with Matrigel. 1×10^5 cells/well MDA-MB-231 cells were cultured in the upper chamber of a 24-well transwell chamber (8 μm pore size, Corning Costar), and the lower surface was treated with **II-19k** with indicated concentrations for 48 h. Cells on the upper surface of the membrane were removed, and cells that migrated or invaded from the lower surface of the membrane were stained with crystal violet. Images of migrating or invasive cells were acquired at the bottom of the chamber, and the number of migrating or invasive cells was counted in at least three fields from random locations.

4.2.11 Wound Healing Assays

HUVEC cells were cultured in 6-well plates for 24 h. Scratch the confluent monolayer of cells with a 200 μL pipette tip. The wounds were then rinsed twice with PBS to remove unadhered cell debris. Add media containing **II-19k** with indicated concentrations to the petri dishes. Cells that migrated through the wound were photographed at 0 h and 24 h by phase contrast microscopy.

4.2.12 Tube Formation Assay

The EC Matrigel matrix was thawed overnight at 4°C, and after polymerizing at 37°C for 0.5 h, HUVECs suspended in F12K were cultured in 96-well culture plates at

a cell density of 50,000 cells/well. Treated with 20 μL of different concentrations of **II-19k** or vehicle at 37 °C for 6 h, cell morphology and tube formation were observed and photographed under an inverted microscope (OLYMPUS, Japan).

4.2.13 In Vivo Antitumor Assay

Animal experiments were performed with institutional approval in accordance with the NIH Guide for the Care and Use of Laboratory Animals. Female ICR mice (4~5 weeks old, 18-22 g, obtained from Shanghai Slack Laboratory Animal Co., LTD) were housed at room temperature, and fed standard rodent chow and water. According to the tumor transplantation protocol, 1×10^6 H22 cells were subcutaneously inoculated on the right flank of ICR mice. After one day of incubation, the mice were weighed and randomly divided into 5 groups with six animals in each group. When the tumor volume reached ~100 mm^3, the groups treated with **II-19k**, **8**, and SAHA were administered in a vehicle of 10% DMSO/2% Tween 80/88% saline, respectively. The negative control group was intravenously injected with 10% DMSO/2% Tween 80/88% saline. **II-19k** and **8** were injected intravenously at the frequency of one dose daily for 17 consecutive days; the positive group was given SAHA 25 mg/kg intraperitoneal injection once a day. The body weight and tumor volume were measured every 2 days. All the mice were sacrificed and weighed after treatment. The tumor volume was determined using the following formula: tumor volume $= L \times W^2/2$, where L is the length and W is the width. Tumor inhibition rate (%) = (1-average tumor weight of treatment group/average tumor weight of control group) $\times$ 100%.

4.2.14 Immunohistochemistry Assay

Hematoxylin and eosin (H&E) staining was used for pathological staining of tissues and organs. Major organs including heart, liver, spleen, lung, and kidney were isolated from mice, then fixed with 4% paraformaldehyde, dehydrated, and embedded in paraffin. Section the tissue to a thickness of 4 mm in the vertical plane. After dewaxing, the sections were stained with Mayer hematoxylin stain solution for 5 min, then stained with eosin-phenoxine staining solution for 2 min, and then dehydrated and fixed with neutral resin. The tissue morphology was observed under a microscope.

Mice tissue sections (control and **II-19k**-treated groups at 20 mg/kg in *in vivo*

antitumor experiments) were embedded in paraffin, cut into 4 μm sections, deparaffinized, and treated with citrate buffer. Then, they were blocked with avidin/biotin for 20 minutes. Slides were incubated with CD31 overnight at 4°C. The slides were then treated with horseradish peroxidase goat anti-rabbit secondary antibody for 1 to 3 h and developed with 3,3-diaminobenzidine. Finally, the slides were counterstained with hematoxylin. The mean microvessel density (MVD) was measured by calculating the CD31 positive cells in randomly selected areas in each section using image analysis software and then analyzed with OriginPro 8.0 software.

Reference

[1] D. Hanahan, Hallmarks of Cancer: New Dimensions, Cancer Discovery, 12 (2022) 31-46.

[2] D. Hanahan, Robert A. Weinberg, Hallmarks of Cancer: The Next Generation, Cell, 144 (2011) 646-674.

[3] D. Hanahan, R.A. Weinberg, The Hallmarks of Cancer, Cell, 100 (2000) 57-70.

[4] A. Anighoro, J. Bajorath, G. Rastelli, Polypharmacology: Challenges and Opportunities in Drug Discovery, Journal of Medicinal Chemistry, 57 (2014) 7874-7887.

[5] R. Morphy, C. Kay, Z. Rankovic, From Magic Bullets to Designed Multiple Ligands, Drug Discovery Today, 9 (2004) 641-651.

[6] R. Morphy, Z. Rankovic, Designed Multiple Ligands. An Emerging Drug Discovery Paradigm, Journal of Medicinal Chemistry, 48 (2005) 6523-6543.

[7] A. Kabir, A. Muth, Polypharmacology: The Science of Multi-targeting Molecules,

Pharmacological Research, 176 (2022) 106055.

[8] W. Shuai, G. Wang, Y. Zhang, F. Bu, S. Zhang, D.D. Miller, W. Li, L. Ouyang, Y. Wang, Recent Progress on Tubulin Inhibitors with Dual Targeting Capabilities for Cancer Therapy, Journal of Medicinal Chemistry, 64 (2021) 7963-7990.

[9] K.J. Falkenberg, R.W. Johnstone, Histone Deacetylases and their Inhibitors in Cancer, Neurological Diseases and Immune Disorders, Nature Reviews Drug Discovery, 13 (2014) 673-691.

[10] S. Minucci, P.G. Pelicci, Histone Deacetylase Inhibitors and the Promise of Epigenetic (and more) Treatments for Cancer, Nature Reviews Cancer, 6 (2006) 38-51.

[11] M. Slingerland, H.-J. Guchelaar, H. Gelderblom, Histone Deacetylase Inhibitors: An Overview of the Clinical Studies in Solid Tumors, Anti-Cancer Drugs, 25 (2014) 140-149.

[12] A. Suraweera, K.J. O'Byrne, D.J. Richard, Combination Therapy with Histone Deacetylase Inhibitors (HDACi) for the Treatment of Cancer: Achieving the Full Therapeutic Potential of HDACi, Frontiers in Oncology, 8 (2018) 92.

[13] Q. Liu, B. Hao, M. Zhang, Z. Liu, Y. Huang, X. Zhao, H. Hu, M. Tan, J.-Y. Xu, An Integrative Proteome-Based Pharmacologic Characterization and Therapeutic Strategy Exploration of SAHA in Solid Malignancies, Journal of Proteome Researh, 21 (2022) 953-964.

[14] H. Zhu, Y. Tan, C. He, Y. Liu, Y. Duan, W. Zhu, T. Zheng, D. Li, J. Xu, D.-H. Yang, Z.-S. Chen, S. Xu, Discovery of a Novel Vascular Disrupting Agent Inhibiting Tubulin Polymerization and HDACs with Potent Antitumor Effects, Journal of Medicinal Chemistry, 65 (2022) 11187-11213.

[15] X. Peng, J. Chen, L. Li, Z. Sun, J. Liu, Y. Ren, J. Huang, J. Chen, Efficient Synthesis and Bioevaluation of Novel Dual Tubulin/Histone Deacetylase 3 Inhibitors as Potential Anticancer Agents, Journal of Medicinal Chemistry, 64 (2021) 8447-8473.

[16] Y. Wang, M. Sun, Y. Wang, J. Qin, Y. Zhang, Y. Pang, Y. Yao, H. Yang, Y. Duan, Discovery of Novel Tubulin/HDAC Dual-target Inhibitors with Strong Antitumor and Antiangiogenic Potency, European Journal of Medicinal Chemistry, 225 (2021) 113790.

[17] C. Hauguel, S. Ducellier, O. Provot, N. Ibrahim, D. Lamaa, C. Balcerowiak, B.

Letribot, M. Nascimento, V. Blanchard, L. Askenatzis, H. Levaique, J. Bignon, F. Baschieri, C. Bauvais, G. Bollot, D. Renko, A. Deroussent, B. Prost, M.-C. Laisne, S. Michallet, L. Lafanechère, S. Papot, G. Montagnac, C. Tran, M. Alami, S. Apcher, A. Hamze, Design, Synthesis and Biological Evaluation of Quinoline-2-carbonitrile-based Hydroxamic Acids as Dual Tubulin Polymerization and Histone Deacetylases Inhibitors, European Journal of Medicinal Chemistry, 240 (2022) 114573.

[18] Y.-R. Li, F.-F. Liu, W.-B. Liu, Y.-F. Zhang, X.-Y. Tian, X.-J. Fu, Y. Xu, J. Song, S.-Y. Zhang, A Novel Aromatic Amide Derivative SY-65 Co-targeted Tubulin and Histone Deacetylase 1 with Potent Anticancer Activity In Vitro and In Vivo, Biochemical Pharmacology, 201 (2022) 115070.

[19] T. Mühlethaler, D. Gioia, A.E. Prota, M.E. Sharpe, A. Cavalli, M.O. Steinmetz, Comprehensive Analysis of Binding Sites in Tubulin, Angewandte Chemie International Edition, 60 (2021) 13331-13342.

[20] M.O. Steinmetz, A.E. Prota, Microtubule-Targeting Agents: Strategies To Hijack the Cytoskeleton, Trends in Cell Biology, 28 (2018) 776-792.

[21] C. Dumontet, M.A. Jordan, Microtubule-binding Agents: A Dynamic Field of Cancer Therapeutics, Nature Reviews Drug Discovery, 9 (2010) 790-803.

[22] E.C. McLoughlin, N.M. O'Boyle, Colchicine-Binding Site Inhibitors from Chemistry to Clinic: A Review, Pharmaceuticals, 13 (2020) 8.

[23] W. Li, H. Sun, S. Xu, Z. Zhu, J. Xu, Tubulin Inhibitors Targeting the Colchicine Binding Site: A Perspective of Privileged Structures, Future Medicinal Chemistry, 9 (2017) 1765-1794.

[24] G.Ş. Karatoprak, E. Küpeli Akkol, Y. Genç, H. Bardakcı, Ç. Yücel, E. Sobarzo-Sánchez, Combretastatins: An Overview of Structure, Probable Mechanisms of Action and Potential Applications, Molecules, 25 (2020) 2560.

[25] S. Paidakula, S. Nerella, S. Kankala, K.R. Kankala, Recent Trends in Tubulin-Binding Combretastatin A-4 Analogs for Anticancer Drug Development, Current Medicinal Chemistry, 29 (2022) 3748-3773.

[26] K. Guo, X. Ma, J. Li, C. Zhang, L. Wu, Recent Advances in Combretastatin A-4 Codrugs for Cancer Therapy, European Journal of Medicinal Chemistry, 241 (2022)

114660.

[27] S. Messaoudi, B. Tréguier, A. Hamze, O. Provot, J.-F. Peyrat, J.R. De Losada, J.-M. Liu, J. Bignon, J. Wdzieczak-Bakala, S. Thoret, J. Dubois, J.-D. Brion, M. Alami, Isocombretastatins A versus Combretastatins A: The Forgotten isoCA-4 Isomer as a Highly Promising Cytotoxic and Antitubulin Agent, Journal of Medicinal Chemistry, 52 (2009) 4538-4542.

[28] I. Khelifi, T. Naret, D. Renko, A. Hamze, G. Bernadat, J. Bignon, C. Lenoir, J. Dubois, J.-D. Brion, O. Provot, M. Alami, Design, Synthesis and Anticancer Properties of IsoCombretaQuinolines as Potent Tubulin Assembly Inhibitors, European Journal of Medicinal Chemistry, 127 (2017) 1025-1034.

[29] W. Li, W. Shuai, H. Sun, F. Xu, Y. Bi, J. Xu, C. Ma, H. Yao, Z. Zhu, S. Xu, Design, Synthesis and Biological Evaluation of Quinoline-indole Derivatives as Anti-Tubulin Agents Targeting the Colchicine Binding Site, European Journal of Medicinal Chemistry, 163 (2019) 428-442.

[30] Yang, Z.; Wang, T.; Wang, F.; Niu, T.; Liu, Z.; Chen, X.; Long, C.; Tang, M.; Cao, D.; Wang, X.; Xiang, W.; Yi, Y.; Ma, L.; You, J.; Chen, L. Discovery of Selective Histone Deacetylase 6 Inhibitors Using the Quinazoline as the Cap for the Treatment of Cancer. Journal of Medicinal Chemistry, 59 (2016) 1455-1470.

[31] Weng, H.; Li, J.; Zhu, H.; Wong, K. F. C.; Zhu, Z.; Xu, J. An Update on the Recent Advances and Discovery of Novel Tubulin Colchicine Binding Inhibitors. Future Medicinal Chemistry, 15 (2023) 73-95.

[32] He, X.; Hui, Z.; Xu, L.; Bai, R.; Gao, Y.; Wang, Z.; Xie, T.; Ye, X. Y. Medicinal Chemistry Updates of Novel HDACs Inhibitors (2020 to present). European Journal of Medicinal Chemistry, 227 (2022) 113946.

[33] Sinha, K.; Das, J.; Pal, P. B.; Sil, P. C. Oxidative Stress: the Mitochondria-Dependent and Mitochondria-Independent Pathways of Apoptosis. Archives of Toxicology, 87 (2013) 1157-1180.

[34] Waris, G.; Ahsan, H. Reactive Oxygen Species: Role in the Development of Cancer and Various Chronic Conditions. Journal of Carcinogenesis, 5 (2006) 14.

[35] Zimmermann, M.; Box, C.; Eccles, S. A. Two-Dimensional vs. Three-Dimensional

in vitro Tumor Migration and Invasion Assays. Methods in Molecular Biology, 986 (2013) 227-252.

[36] Li, X.; Li, Y.; Lu, W.; Chen, M.; Ye, W.; Zhang, D. The Tumor Vessel Targeting Strategy: A Double-Edged Sword in Tumor Metastasis. Cells, 8 (2019) 1602.